Department of Micro- and Nanosciences

Reducing surface recombination in black silicon photovoltaic devices using atomic layer deposition

Päivikki Repo

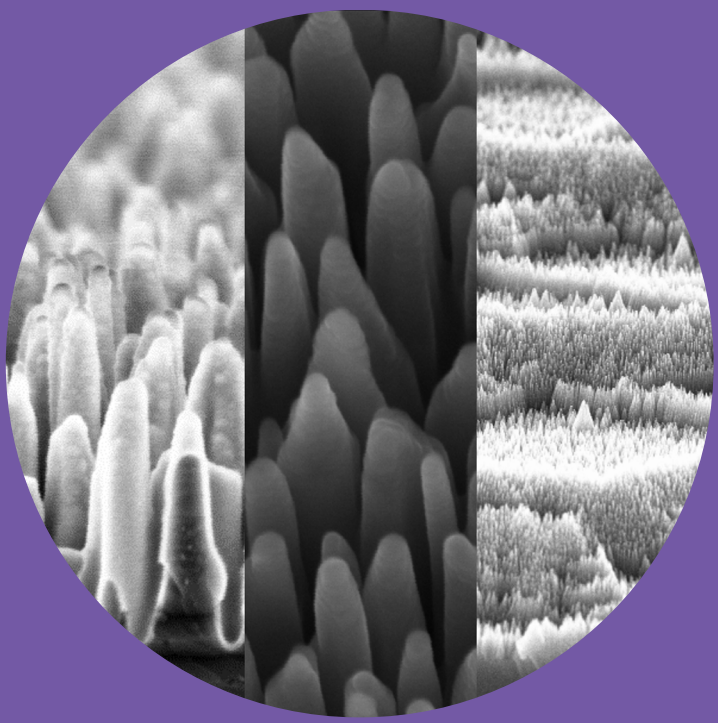

Aalto University

DOCTORAL DISSERTATIONS

Aalto University publication series
DOCTORAL DISSERTATIONS 139/2016

Reducing surface recombination in black silicon photovoltaic devices using atomic layer deposition

Päivikki Repo

A doctoral dissertation completed for the degree of Doctor of Science (Technology) to be defended, with the permission of the Aalto University School of Electrical Engineering, at a public examination held in the Large Seminar Hall of Micronova on the 9th of September 2016 at 12 noon.

Aalto University
School of Electrical Engineering
Department of Micro- and Nanosciences
Electron Physics Group

Supervising professor
Prof. Hele Savin

Preliminary examiners
Prof. Erik Stensrud Marstein, University of Oslo, Norway
Dr. Paul R. Coxon, University of Cambridge, United Kingdom

Opponent
Prof. Stefan Glunz, University of Freiburg, Germany

Aalto University publication series
DOCTORAL DISSERTATIONS 139/2016

ISBN 978-952-60-6918-0 (printed)
ISBN 978-952-60-6919-7 (pdf)
ISSN-L 1799-4934
ISSN 1799-4934 (printed)
ISSN 1799-4942 (pdf)
http://urn.fi/URN:ISBN:978-952-60-6919-7

Unigrafia Oy
Helsinki 2016

Finland

441 697
Printed matter

Aalto University

Abstract

Aalto University, P.O. Box 11000, FI-00076 Aalto www.aalto.fi

Author
Päivikki Repo

Name of the doctoral dissertation
Reducing surface recombination in black silicon photovoltaic devices using atomic layer deposition

Publisher School of Electrical Engineering

Unit Department of Micro- and Nanosciences

Series Aalto University publication series DOCTORAL DISSERTATIONS 139/2016

Field of research Semiconductor Technology

Manuscript submitted 22 April 2016 **Date of the defence** 9 September 2016

Permission to publish granted (date) 20 June 2016 **Language** English

☐ **Monograph** ☒ **Article dissertation** ☐ **Essay dissertation**

Abstract

Surface recombination in silicon solar cells decreases the collection probability of charge carriers and can hence lower the cell efficiency significantly. The reduction of this detrimental effect is addressed in this work by passivating the surface with different atomic layer deposited (ALD) thin film coatings. It is shown that surface passivation with aluminum oxide (Al_2O_3) or hafnium oxide (HfO_2) is dependent on the oxidant used in the ALD process. Higher deposition temperatures lead to better surface passivation with aluminum nitride (AlN) films where carrier lifetimes of more than 1 ms can be reached with additional corona charge. In general, all of the thin films studied here provide good surface passivation with low values for interface defect density.

Surface passivation becomes even more important in the case of black silicon (b-Si), *i.e.* nanostructured silicon surface, where the large surface area results in high surface recombination velocity. Black silicon itself has gained much interested especially for photovoltaic applications due to its low surface reflectance on a wide spectral range and acceptance angle. However, the increase in the surface recombination has always hindered the application of b-Si *e.g.* in solar cells. This work presents that ALD Al_2O_3 can solve this issue by providing completely conformal coating and excellent passivation also on nanostructured surfaces. In addition to surface passivation, Al_2O_3 coating further reduces the reflectance leading to values less than 1 % on the whole spectral range relevant for solar cell operation.

As good surface passivation is reached on b-Si, its applicability on different photovoltaic devices including two types of solar cells and a photodiode is demonstrated. First, it is shown that different emitter diffusion processes do not hinder the optical properties of black silicon and that excellent surface passivation is also reached on boron doped emitters using ALD Al_2O_3. This discovery is then applied in the fabrication of n-type front contact solar cells with b-Si and Al_2O_3 passivation on the front surface and an efficiency of 18.7 % is reached. Even higher efficiencies of 22.1 % are gained with back contact solar cells. This is so far the highest efficiency reached with black silicon solar cells. Finally, Al_2O_3 surface passivation and black silicon are applied on induced junction photodiodes and external quantum efficiency of 96 % is reached on the measured wavelength range of 250-950 nm. This proves that the use of b-Si and Al_2O_3 surface passivation is not limited only to solar cells but also other optoelectronic applications can benefit from it.

Keywords black silicon, atomic layer deposition, surface passivation, photovoltaic devices

ISBN (printed) 978-952-60-6918-0 **ISBN (pdf)** 978-952-60-6919-7

ISSN-L 1799-4934 **ISSN (printed)** 1799-4934 **ISSN (pdf)** 1799-4942

Location of publisher Helsinki **Location of printing** Helsinki **Year** 2016

Pages 122 **urn** http://urn.fi/URN:ISBN:978-952-60-6919-7

Tekijä
Päivikki Repo

Väitöskirjan nimi
Mustaa piitä hyödyntävien valosähköisten komponenttien pintarekombinaation vähentäminen atomikerroskasvatuksen avulla

Julkaisija Sähkötekniikan korkeakoulu

Yksikkö Mikro- ja nanotekniikan laitos

Sarja Aalto University publication series DOCTORAL DISSERTATIONS 139/2016

Tutkimusala Puolijohdeteknologia

Käsikirjoituksen pvm 22.04.2016 **Väitöspäivä** 09.09.2016

Julkaisuluvan myöntämispäivä 20.06.2016 **Kieli** Englanti

☐ **Monografia** ☒ **Artikkeliväitöskirja** ☐ **Esseeväitöskirja**

Tiivistelmä

Piiaurinkokennojen pintarekombinaatio pienentää varauksenkuljettajien keräystodennäköisyyttä ja voi näin ollen laskea aurinkokennojen hyötysuhdetta. Tämän epäsuotuisan ilmiön vähentämistä tutkitaan tässä työssä passivoimalla piin pinta erilaisilla atomikerroskasvatetuilla (ALD) ohutkalvoilla. Pintapassivoinnin laatu alumiinioksidilla (Al_2O_3) tai hafniumoksidilla (HfO_2) riippuu ALD-prosessissa käytettävästä oksidantista. Alumiininitridin (AlN) tapauksessa korkeampi kasvatuslämpötila johtaa parempaan pintapassivointiin ja yli 1 ms:n elinaika on saavutettavissa lisäämällä koronavarausta kiekkojen pinnalle. Kokonaisuudessaan kaikki tässä työssä tutkitut ohutkalvot takaavat hyvän pintapassivoinnin ja hyvälaatuisen ohutkalvo/pii -rajapinnan.

Pintapassivoinnin roolista tulee vielä suurempi mustan piin (nanokuvioitu piin pinta) tapauksessa suuremman pinta-alan johtaessa korkeampaan pintarekombinaationopeuteen. Musta pii on herättänyt mielenkiintoa erityisesti potentiaalisena aurinkokennojen etupinnan kuviointina, koska se vähentää pintaheijastusta laajalla aallonpituusalueella ja myös suurilla tulokulmilla. Hyöty matalasta pintaheijastuksesta on kuitenkin jäänyt vähäiseksi suuren pintarekombinaation vuoksi. Tässä työssä osoitetaan, että konformaalinen ALD alumiinioksidi voi ratkaista mustan piin pintapassivointiongelman. Erinomaisen pintapassivoinnin lisäksi Al_2O_3 laskee jo valmiiksi matalaa heijastusta entisestään: alle 1 %:n heijastus saavutetaan koko aurinkokennoille merkityksellisellä aallonpituusalueella.

Koska pintapassivointiongelma on saatu ratkaistua, testataan mustan piin toimivuutta myös erilaisissa valosähköisissä komponenteissa mukaan lukien kaksi aurinkokennoa ja valodiodi. Ensimmäiseksi osoitetaan, ettei emitteridiffuusio heikennä mustan piin optisia ominaisuuksia ja että myös korkeasti boorilla seostettu mustan piin pinta saadaan tehokkaasti passivoitua alumiinioksidilla. Tätä tietoa hyödynnetään n-tyypin etukontaktikennojen valmistuksessa, joiden etupinnalla on mustaa piitä ja Al_2O_3-kalvo. Näillä kennoilla saavutetaan 18.7 %:n hyötysuhde. Vielä korkeampi hyötysuhde – 22.1 % – saavutetaan takakontaktikennoilla. Lopuksi mustan piin ja ALD Al_2O_3 -passivoinnin yhdistelmää hyödynnetään valodiodissa, jolla saavutetaan yli 96 %:n kvanttihyötysuhde koko mitatulla spektrialueella (250-950 nm). Tämä osoittaa, että mustan piin ja ALD Al_2O_3 passivoinnin yhdistelmän soveltuvuus ei rajoitu ainoastaan aurinkokennoihin, vaan potentiaalisia käyttökohteita ovat myös muut optoelektroniikan sovellukset.

Avainsanat musta pii, atomikerroskasvatus, pintapassivointi, valosähköinen komponentti

ISBN (painettu) 978-952-60-6918-0 **ISBN (pdf)** 978-952-60-6919-7

ISSN-L 1799-4934 **ISSN (painettu)** 1799-4934 **ISSN (pdf)** 1799-4942

Julkaisupaikka Helsinki **Painopaikka** Helsinki **Vuosi** 2016

Sivumäärä 122 **urn** http://urn.fi/URN:ISBN:978-952-60-6919-7

Preface

The research presented in this thesis was carried out at the Department of Micro- and Nanosciences at Aalto University School of Electrical Engineering and at the Department of Solar Cells - Development and Characterization at Fraunhofer Institute for Solar Energy Systems. The list of people that I am in debt to has grown long and although time and chemical fumes have weakened my memory I hope most of them are listed below. First, I would like to express my gratitude to Prof. Hele Savin for giving me the opportunity to work in the Electron Physic Group. Her help and guidance throughout this work has been indispensable. Emeritus Prof. Pekka Kuivalainen hired me to do my master's thesis at EPG all those years ago and for that I am grateful. I would also like to thank Prof. Stefan Glunz for honoring me by being my opponent and Prof. Erik Stensrud Marstein and Dr. Paul R. Coxon for the pre-examination of this work.

I would like to thank the past and present members of the whole Electron Physics Group, especially all my co-authors. I've had the questionable privilege of sharing an office with Dr. Ville Vähänissi from the day I started working at EPG. Thank you and my apologies. I'm grateful to Heli Talvitie for all the help and guidance in the cleanroom (and also for the map of Freiburg). The advice from Antti Haarahiltunen and Marko Yli-Koski has always been valuable to all of EPG. A thank you goes to Lauri Sainiemi for helping us to get started our work regarding black silicon which is the corner stone of this thesis and of the many more to come. I would like to thank Alexander Perros, Perttu Sippola and Ali Shah as well as Esa Tuovinen for their help with ALD, ICP and whatever processes you can think of. Thank you goes also to the research assistants Heli Seppänen and Toni Pasanen who have helped me with the sometimes overwhelming workload in the cleanroom. Micronova cleanroom and other facilities would not function without the expertise of Nanofab personnel, past and present. Thank you.

I'm thankful to the researches from UPC in Barcelona – Pablo, Ramon, Moises and Eric - for giving me the opportunity to be part of fabricating one of the best black silicon solar cells to date. It would have been impossible without you.

I would like to express my gratitude to Martin Schubert and Jan Benick from Fraunhofer ISE who both guided me during my stay there. Special thanks goes to the whole Characterization group at that time, especially Florian, Jan, Jonas and Tim. You are an intimidatingly smart group of people and great friends. Johannes Giesecke from ISE showed considerable patience for both my company and my stupid questions and for that he would deserve a medal. Thank you goes also to Bernd Steinhauser and the cleanroom and characterization personnel at ISE who with great care and patience fabricated our solar cells.

I am forever grateful to all of my friends, especially Emilia who has been there since the day we started together at the university and Satu who, in addition to everything else, terrorized also the writing process of this thesis. My deepest gratitude goes to Laura and Herr Dr. Freddie. It seems I cannot get rid of you people even by moving back to Finland.

My parents have supported me throughout my life and a thank you is in order, however insufficient it is. My sisters Kaisa and Eveliina made this whole PhD stuff a trend in our family and I blame them for pushing me down the rabbit hole six years ago. It has always been a pleasure to have you as my sisters. I also want to thank my brother Pekka as he helped me pass the basic course in programming (it never was my strong subject). My last and utmost gratitude goes to my significant other Sami for bearing with me. I know it's not easy.

Espoo, July 2016

Päivikki Repo

"Well that was the silliest tea party I ever went to!
I am never going back there again!"
– Lewis Carroll, Alice in Wonderland

Contents

List of publications

This thesis consists of an overview of the following seven publications. They are from here on referred in the text with their Roman numerals:

I P. Repo, H. Talvitie, S. Li, J. Skarp, and H. Savin, Silicon surface passivation by Al_2O_3: effect of ALD reactants, *Energy Procedia* 8, p. 681-687 (2011).

II P. Repo, Y. Bao, H. Seppänen, P. Sippola, and H. Savin, Silicon surface passivation with atomic layer deposited aluminum nitride, *Accepted for publication in the Proceedings of the 43rd IEEE Photovoltaic Specialists Conference.*

III P. Repo, A. Haarahiltunen, L. Sainiemi, M. Yli-Koski, H. Talvitie, M. C. Schubert, and H. Savin, Effective passivation of black silicon surfaces by atomic layer deposition, *Journal of Photovoltaics* 3, p. 90-94 (2013).

IV P. Repo and H. Savin, Effect of different ALD Al_2O_3 oxidants on surface passivation of black silicon, *Accepted for publication in Energy Procedia*.

V P. Repo, J. Benick, G. von Gastrow, V. Vähänissi, F. D. Heinz, J. Schön, M. C. Schubert, and H. Savin, Passivation of black silicon boron emitters with atomic layer deposited aluminum oxide, *Physica Status Solidi Rapid Research Letters* 7, p. 950-954 (2013).

VI P. Repo, J. Benick, V. Vähänissi, J. Schön, G. von Gastrow, B. Steinhauser, M. C. Schubert, M. Hermle, and H. Savin, N-type black silicon solar cells, *Energy Procedia* 38, p. 866-871 (2013).

VII H. Savin, P. Repo, G. von Gastrow, P. Ortega, E. Calle, M. Garín, and R. Alcubilla, Black silicon solar cells with interdigitated back-contacts achieve 22.1% efficiency, *Nature Nanotechnology* 10, p. 624-628 (2015).

Author's contribution

I The author participated in sample processing, measurements and data analysis. The author prepared the manuscript.

II The author planned the experiments and participated actively in sample processing and measurements. The author analyzed the data and prepared the manuscript.

III The author participated actively in sample processing and measurements. The author participated in analyzing the data and prepared the manuscript.

IV The author planned the experiments and processed and measured the samples. The author analyzed the data and prepared the manuscript.

V The author participated actively in planning the experiments, performed the reflectance and J_{0e} measurements, participated in analyzing the data and prepared the manuscript.

VI The author participated actively in planning the experiments and analyzing the data. The author prepared the manuscript.

VII The author participated actively in planning the experiments, sample processing and manuscript preparation.

Abbreviations

Al	Aluminum
ALD	Atomic layer deposition
Al_2O_3	Aluminum oxide
AlN	Aluminum nitride
a-Si:H	Hydrogenated amorphous silicon
b-Si	Black silicon
C	Carbon
Cl	Chlorine
COCOS	Corona-oxide characterization of semiconductor
Cz-Si	Czochralski silicon
DRIE	Deep reactive ion etching
EQE	External quantum efficiency
F*	Fluorine radical
FF	Fill factor
FGA	Forming gas anneal
FZ-Si	Float Zone silicon
H	Hydrogen
Hf	Hafnium
$HfCl_4$	Hafnium tetrachloride
HfO_2	Hafnium oxide
H_2O	Water
IBC	Interdigitated back-contact
IQE	Internal quantum efficiency
mc-Si	Multicrystalline silicon
µ-PCD	Microwave photoconductance decay
N	Nitrogen
N_2	Nitrogen molecule
NH_3	Ammonia
O*	Oxygen radical
O	Oxygen
O_2	Oxygen molecule
O_3	Ozone
PA-ALD	Plasma-assisted atomic layer deposition
PECVD	Plasma-enhanced chemical vapor deposition
PERL	Passivated emitter with rear locally diffused
PFF	Pseudo-fill factor

PL	Photoluminescence
QSSPC	Quasi-steady state photoconductance
QSSPL	Quasi-steady state photoluminescence
RTA	Rapid thermal anneal
SC2	Standard cleaning solution 2
SEM	Scanning electron microscopy
SF_6	Sulfur hexafluoride
Si	Silicon
SiF_4	Silicon tetrafluoride
SiN_x	Silicon nitride
SiO_x	Silicon oxide
SiO_2	Silicon dioxide
SiO_xF_y	Silicon-oxyfluoride
TDMAH	Tetrakis(dimethylamino)hafnium
Ti	Titanium
$TiCl_4$	Titanium tetrachloride
TiO_2	Titanium oxide
TMA	Trimethylaluminum

Symbols

D_{it}	Interface defect density
I-V	Current-voltage
J-V	Current density-voltage
J_{sc}	Short-circuit current
J_{0e}	Emitter saturation current density
P-V	Power density-voltage
Q_{tot}	Total charge density
R	Reflectance
R_w	Spectrum weighted reflectance
S_{eff}	Surface recombination velocity
$S_{eff,max}$	Maximum surface recombination velocity
T	Temperature
V_{oc}	Open-circuit voltage
$V_{oc,max}$	Maximum open-circuit voltage
$V_{oc,impl}$	Implied open-circuit voltage
W	Wafer thickness
η	Solar cell efficiency
λ	Wavelength
τ_{eff}	Minority carrier lifetime

1. Introduction

Surface recombination in silicon solar cells can significantly lower the cell efficiency. One of the most common ways of reducing surface recombination - *i.e.* surface passivation - is to apply a thin film on the silicon surface. The passivation ability of thin films is based on two separate effects: chemical and field-effect passivation. The former refers to the reduction of dangling bonds whereas field-effect passivation is based on charge in the thin film that, depending on the charge polarity, pushes away either electrons or holes and hence prevents their recombination on the surface. Some of the thin films used for surface passivation can have a second but equally important role: they can also act as antireflection coatings and hence reduce reflective losses.

The applicability of different thin films depends on the doping density and type of the passivated surface as well as the polarity of the fixed charge. In addition, the films should not absorb light in the wavelength region relevant for solar cell operation. Traditional materials for surface passivation of silicon solar cells are thermal SiO_2 and plasma-enhanced chemical vapor deposition (PECVD) SiN_x and a-Si:H [1-3]. However, in recent years different atomic layer deposited (ALD) thin films have gained more and more interest as potential surface passivation materials [4]. With ALD good film quality, accurate thickness control and conformality are reached. A variety of ALD materials have demonstrated good surface passivation quality both for front and rear surface of silicon solar cells, the most studied being Al_2O_3 [5]. Unlike the traditional thin film materials mentioned above, the inherent negative fixed charge of Al_2O_3 makes it applicable also for passivation of p+ surfaces. This has become increasingly important as n-type solar cells have gained more ground in the photovoltaic research and industry [6].

In addition to optimizing the thin film for the best possible surface passivation they can be also optimized to reduce front surface reflectance, as mentioned above. This is done by choosing a material with a suitable refractive index and by adjusting the film thickness. Combining this method with surface texturing, *e.g.* random or inverted pyramids, reflectance can be reduced near zero with a certain wavelength and angle of incidence. In some cases a film stack such as SiO_2/SiN_x is used in order to reach simultaneously good surface passivation and antireflection [7]. From the ALD materials, Al_2O_3 for example does not provide proper antireflection due to its low refractive index whereas TiO_2 and HfO_2 show more promise on that regard [8-9].

Although low reflectances have been reached with the combination of macroscopic surface texturing and antireflection coatings there is still room for improvement, especially as sunlight consists of multiple wavelengths and does not always arrive on the solar cell surface perpendicularly. Nanostructuring of silicon *i.e.* black silicon or b-Si (also nanocones, nanopyramids, nanograss etc.) has been investigated extensively for its ability to reduce reflectance on a wide spectral range and acceptance angle. However, using b-Si

on the front surface of solar cells has always led to a compromise: the gain from the low reflectance has been suppressed by the increase of surface recombination due to large surface area of the nanostructure. The traditional surface passivation materials, namely SiO_2 and SiN_x, have not provided sufficient surface passivation for b-Si mostly due to poor conformality or insufficient field-effect [10] and hence problems related to b-Si surface recombination have remained unresolved.

The main goal of this thesis is to study if the surface recombination issue of b-Si can be solved with ALD Al_2O_3 coating. ALD has superior conformality as compared to other thin film deposition methods enabling the deposition of uniform films also on nanostructured surfaces [11]. Hence, from this perspective Al_2O_3 and other ALD thin film materials have the potential of providing good passivation on black silicon surfaces. Although this study is driven by the potential advantages b-Si has for solar cells other applications might benefit as well. For example in photodiodes, low reflectance could enable the detection of smaller amounts of light and good surface passivation could provide better light response.

First, surface passivation is studied on planar surfaces with different ALD thin film materials including Al_2O_3, AlN and HfO_2 and the results are summarized in Chapter 2 (Publications I and II). Both AlN and HfO_2 have a high refractive index and therefore they could also be used as efficient antireflection coatings. In the study of Al_2O_3 and HfO_2 the focus is on the effect of different ALD oxidants on the surface passivation quality of the respective thin films whereas for AlN different growth temperatures and postdeposition heat treatments are tested. In Chapter 3 surface passivation of black silicon with ALD Al_2O_3 is discussed (Publication III). More specifically, the effect of using different ALD oxidants on the surface passivation of lowly doped b-Si is presented (Publication IV). As the first step towards actual solar cells, different boron diffusion processes are applied on black silicon to see their effect on the optical properties and to investigate if also b-Si emitters can be passivated with Al_2O_3 (Publication V). In Chapter 4 black silicon is applied on final devices including front and rear contact solar cells and photodiodes (Publications VI and VII).

2. Silicon surface passivation with atomic layer deposited thin films

2.1 Atomic layer deposition

Atomic layer deposition (ALD) is a thin film growth method based on two half reactions as presented in Figure 1. First, the surface is introduced with the first precursor that reacts with the surface. Then the unreacted precursor and the reaction byproducts are swept away with a purge step *i.e.* a flow of inert gas such as nitrogen. Then, the second precursor is introduced so it can react with the surface, followed by a purge step. This entity is referred to as ALD cycle and it is repeated as many times as needed to reach the desired film thickness. The two half cycles of different precursors create the desired material on the surface without reacting in the gas phase making sure that ALD is purely a surface controlled process. The fact that no reaction should take place in the gas phase is the key for atomic level thickness control and the good quality of the films. It also separates ALD from other thin film growth methods such as sputtering or plasma-enhanced chemical vapor deposition (PECVD) where precursors reside in the reaction chamber simultaneously. In addition to the thickness control, thin films grown with ALD are pin hole free and the conformality of the films is better than can be reached with any other thin film deposition method.

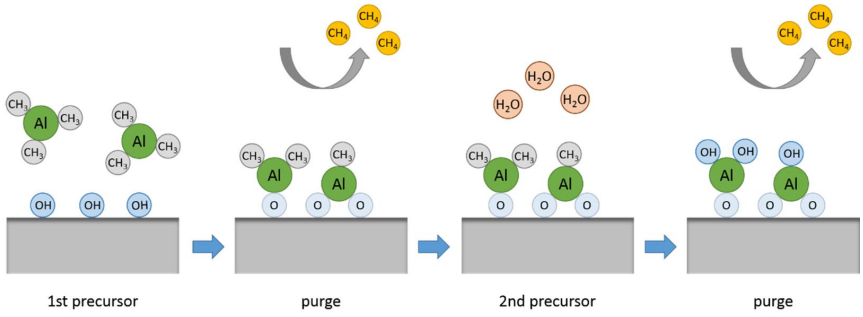

Figure 1. *ALD process cycle for aluminum oxide consisting of two precursor (trimethylaluminum and water) and two purge steps. During the purge step the ALD reactor is emptied from reaction byproducts and unreacted precursor. After the second purge step the first precursor is introduced again into the reactor and the process is continued until the desired film thickness is reached.*

2.2 Aluminum oxide

Efficient front and rear surface passivation is of vital importance for the operation of silicon solar cells. Without proper surface passivation, charge carriers recombine and do not contribute to the collected current, lowering the solar cell efficiency. Surface passivation can be implemented with different types of thin films deposited or grown on the silicon

surface. Thin films passivate the surface due to two effects: 1) chemical passivation *i.e.* reduction of dangling bonds and 2) field-effect passivation due to a charge in the thin film. Traditional materials for this are PECVD SiN_x [1] and a-Si:H [2] as well as thermal SiO_2 [3]. These thin films have inherent positive fixed charge and hence they provide good surface passivation for p and n-type as well as highly doped n+ surfaces. As n-type silicon as the base material for solar cells has gained more and more interest also a method for p+ emitter passivation has been required. Since Al_2O_3 possesses a negative fixed charge it has become a potential material to solve this issue [12-13]. In recent years it has been widely recognized that ALD Al_2O_3 provides excellent surface passivation for lightly doped p and n as well as highly doped p+ surfaces [4]. Hoex et al. have also demonstrated that Al_2O_3 can be used for n+ surface passivation on a certain sheet resistance range [14]. Fixed negative charge values of $(2–13)\times10^{12}$ cm^{-2} and interface defect densities of 1×10^{11} $eV^{-1}cm^{-2}$ are typical for Al_2O_3 films leading to surface recombination velocities less than 5 cm/s [4].

ALD can be divided into thermal and plasma-assisted processes. There are many studies where Al_2O_3 deposition by these two is compared from the point of view of surface passivation [15-17]. Thermal ALD can be implemented by using *e.g.* H_2O or O_3 as an oxidant while plasma process uses O_2. Trimethylaluminum (TMA) is the most common aluminum source although other precursor options have also been considered [18]. Regarding thermal processes, Al_2O_3 from TMA and H_2O can be considered as the model example of ALD and it is also widely studied for surface passivation purposes. However, using O_3 is known to have certain advantages: it is more reactive and it can be purged from the ALD reactor more easily [19]. Al_2O_3 films grown with O_3 are also known to have less carbon and hydrogen residues [20-21].

In Publication I three different precursor combinations were chosen for thermal ALD to see their effect on the surface passivation quality of Al_2O_3. Two of the processes were pure Al_2O_3 deposited with TMA and O_3 or the combination of H_2O and O_3. In the third process TiO_2 was doped into the TMA+O_3 grown Al_2O_3 film using titanium tetrachloride ($TiCl_4$) as the Ti source and H_2O as the oxidant. This resembles the $(Al_2O_3)_x(TiO_2)_{1-x}$ pseudobinary alloys that are known to passivate p-type Si surfaces [22]. For reference, thermal oxidation was done at 900°C.

Figure 2a shows the effect of different ALD precursors on minority carrier lifetimes as a function of injection level measured with quasi-steady state photoconductance (QSSPC) after postdeposition annealing. Wafers used were low resistivity p-type magnetic Cz-Si (2-5 Ωcm). With all injection levels Al_2O_3 seems to provide better surface passivation than the oxidized reference independent of the ALD precursors. At higher injection levels Auger recombination limits the lifetime values. The decrease in lifetime at low injection is most likely caused by the boron-oxygen complex although in magnetic Cz-Si oxygen

concentration is rather low. When the ALD precursors are compared, TiO_2 addition yields the best passivation within the whole injection range. Al_2O_3 with H_2O+O_3 and pure O_3 seem to be comparable, yet better than thermal oxide. Lifetimes measured with microwave photoconductance decay (μ-PCD) at an injection level of about $3 \cdot 10^{14}$ cm^{-3} are also included in the same figure and they are in agreement with the QSSPC results. μ-PCD maps also confirmed that the passivation by Al_2O_3 was laterally homogeneous.

The same three ALD processes were tested also in n-type Cz-Si wafers and the corresponding minority carrier lifetimes measured with QSSPC are shown in Figure 2b. Again, the Auger limit at higher injection levels is seen. In the low injection regime a decrease in the lifetime should be visible due to enhanced bulk recombination in the inversion layer that is created by the negative charge of Al_2O_3 in n-type silicon [4]. However, no such decrease is visible probably because the measurements do not extend to low enough injection level. The results are somewhat similar to p-type wafers but some differences exist. The measured lifetimes are much higher in general (in ms range) most likely due to better bulk material. Also, Al_2O_3 with pure O_3 results in much lower passivation than the other two ALD processes, even lower than the reference oxidation. In Figure 2b Al_2O_3 with H_2O+O_3 and Al_2O_3/TiO_2 alloy can be seen comparable and lifetimes as high as 8-11 ms are obtained. This corresponds to surface recombination velocities of $S_{eff,max}$ = 1.8-2.5 cm/s if an infinite bulk lifetime is assumed. μ-PCD measurements lead to similar results.

From these results it is clear that the choice of precursors can play a major role in surface passivation quality of thermal ALD Al_2O_3. In general, it seems that Al_2O_3 can provide similar or even better surface passivation quality than thermal oxidation. The best results are reached both in n-type and p-type Cz-Si when Al_2O_3 is doped with TiO_2. The lifetime variation between ALD precursor combinations are most likely related to the differences in the negative fixed charge and interface defect density. Al_2O_3 films deposited by using H_2O+O_3 contain more hydrogen than the films deposited with pure O_3 since H_2O acts as one hydrogen source [21]. During annealing hydrogen can diffuse into the interface and result in better interface quality due to dangling bond passivation. This partly explains why postdeposition heat treatment is needed to activate Al_2O_3 surface passivation. Small amount of blistering (*i.e.* partial delamination of the Al_2O_3 film) was observed in H_2O+O_3 process but none when pure O_3 was used. This is also related to the higher amount of H residues in the H_2O process and the fact that blister formation has been associated with hydrogen outdiffusion from the thin film during annealing [23].

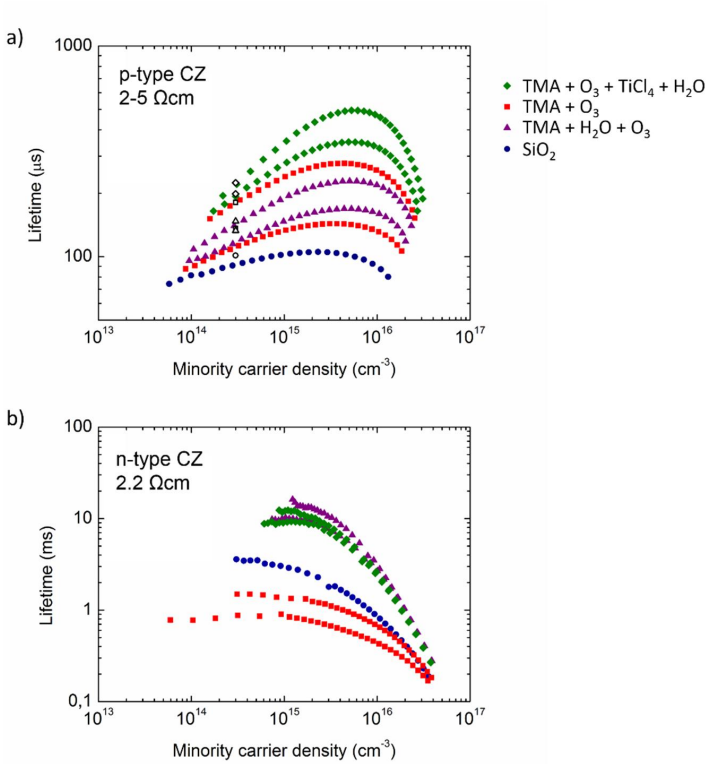

Figure 2. *Carrier lifetimes as a function of minority carrier density measured with QSSPC in a) p-type Cz-Si (2-5 Ωcm) and in b) n-type Cz-Si (2.2 Ωcm) wafers. Al_2O_3 was deposited with three different precursor combinations in the thickness of ~40 nm. Postdeposition anneal was done at 450°C in N_2 for 30 minutes. (Reprinted with permission from P. Repo, H. Talvitie, S. Li, J. Skarp, and H. Savin, Energy Procedia 8, 681-687 (2011). Copyright 2011, Elsevier Ltd.)*

In addition to Al_2O_3 other ALD thin films such as TiO_2 [24], HfO_2 [25], Ga_2O_3 [26] and Ta_2O_5 [27] have shown good silicon surface passivation quality. Different types of film stacks such as SiO_2/Al_2O_3 [28], Al_2O_3/TiO_2 [29] or $Al_2O_3/HfO_2/Al_2O_3$ [30] can be used to optimize the fixed charge and hence surface passivation and simultaneously gain also good antireflection properties. Two other potential ALD materials for surface passivation are discussed in the next chapters.

2.3 Aluminum nitride

Aluminum nitride (AlN) is widely studied in microelectronics and is used in various applications *e.g.* in the electrolyte of dye-sensitized solar cells [31], surface passivating layer on gallium arsenide [32] and insulators for thin film transistors [33]. AlN can have a high refractive index of >1.9 so in addition to surface passivation it could also act simultaneously as an effective antireflection coating [34]. Previous studies on AlN made by reactive ion sputtering have shown that short high temperature treatments form a

moderate fixed negative charge to the film and therefore AlN can provide excellent passivation for both n+ and p+ silicon surfaces [35]. This is a clear benefit as compared to Al_2O_3 that has a high negative charge and hence is not ideal for n+ surface passivation.

In Publication II ALD AlN is introduced as a potential silicon surface passivation material. AlN was grown on low resistivity ~5 Ωcm p-type Cz-Si wafers by plasma-assisted atomic layer deposition (PA-ALD) using TMA and ammonia (NH_3) plasma as precursors. The depositions were made on both sides of the samples at 200°C, 250°C or 300°C leading to deposition rates of 0.7Å/cycle, 0.85Å/cycle and 1.0Å/cycle, respectively. The corresponding refractive indexes were measured with ellipsometer: 1.86, 1.89 and 1.91. The amount of ALD cycles was adjusted according to the growth rates to acquire around 30-40 nm thick AlN film.

AlN does not provide sufficient surface passivation in the as-deposited state as shown in Figure 3a. Hence, different types of postdeposition heat treatments were applied. These include annealing in 450°C for 15 minutes followed by firing in an RTA furnace at ~830-850°C for ~5 seconds. Higher deposition temperature of AlN leads to higher lifetimes and annealing at 450°C increase the lifetime regardless of the deposition temperature. Highest lifetime is reached with highest deposition temperature after annealing and firing. Contactless CV measurements (COCOS) [36] show that the total AlN/Si charge (Q_{tot}) is already negative in the as-deposited state at a deposition temperature of 300ºC (see Figure 3b). With lower temperatures the charge is positive and only after heat treatment becomes negative. In all cases annealing clearly increases the negative charge and after the heat treatment sequence the charge values are in the same level. Krugel et al. suggest that the fixed charge formation in AlN is due to diffusion of Al or changes in the atomic configuration [35]. Al vacancy is negatively charged and the same applies to the combination of an Al and N vacancy $(V_{Al}\text{-}V_N)^{-1}$ that can be formed at elevated temperatures [37]. Negative charge in the as-deposited 300ºC samples could be explained by the formation of $(V_{Al}\text{-}V_N)^{-1}$ vacancies already during deposition due to sufficiently high temperature.

Higher deposition temperature leads to clearly lower initial interface defect density (D_{it}) as shown in Figure 3c. Annealing increases the D_{it} values which are then reduced by a firing step. This change is within the error limits of D_{it} extraction by COCOS measurements that has been stated to be around 20% [38]. In samples that were processed at 200°C the measurements exhibit a large error and hence these results are excluded from Figure 3c. The measurements however indicate that the D_{it} in the 200°C processed samples is higher than in the samples processed at higher temperatures in all cases, *i.e.* as-deposited or heat treated. This could also explain the low lifetimes in the samples deposited at 200°C.

The best surface passivation with the 300°C deposition temperature is consistent with the Q_{tot} and D_{it} values: highest charge and lowest defect density are reached with this

process. Although sufficient level of surface passivation with AlN is reached, further optimization of the process *e.g.* by adjusting the H concentration in AlN could still improve the passivation quality. However, the process presented here could already be tested for p+ and n+ surface passivation as the interface quality, *i.e.* chemical passivation, is good and the charge is in a moderate level. More than 1 ms lifetime ($S_{eff,max}$ ~28 cm/s) was reached in the samples processed at 300°C after corona charge addition on both wafer surfaces. This further proves the excellent AlN/Si interface quality.

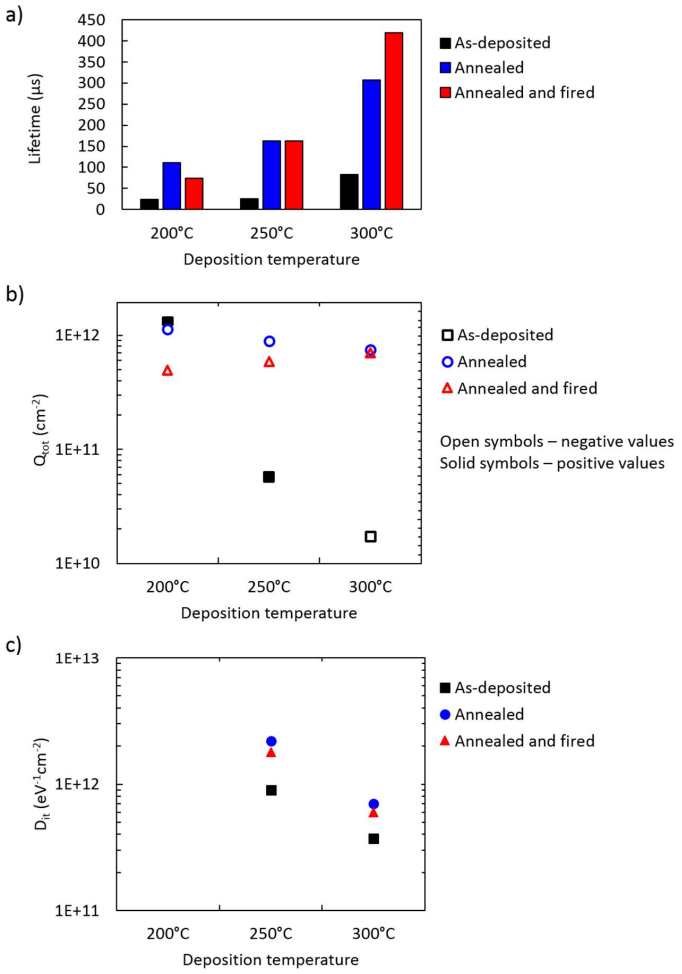

Figure 3. *a) Minority carrier lifetime at 1 sun, b) total charge density and c) interface defect density of AlN passivated samples before and after heat treatments when different deposition temperatures are used. Samples were first annealed at 450°C for 15 min followed by 830-850°C for 5 s, both in N_2 ambient. Prior to ALD, SC2 cleaning was applied to have a thin chemical oxide on the surface. Open symbols in b) refer to negative and solid symbols to positive values. Lifetimes were measured with µ-PCD at the injection level of 1 sun.*

2.4 Hafnium oxide

The growth of hafnium oxide (HfO_2, hafnia) with ALD has been studied widely because it can replace thermal SiO_2 as the gate dielectric in MOSFETs [39]. Similarly as AlN, HfO_2 can have a high refractive index of ~2 and hence it could be used simultaneously for surface passivation and antireflection in silicon solar cells. The results regarding HfO_2 surface passivation seem to vary depending *e.g.* on the ALD process used. Lin et al. have demonstrated good surface passivation with as-deposited HfO_2 films ($S_{eff,max}$ = 54 cm/s) and that the postdeposition anneal can improve it further ($S_{eff,max}$ = 24 cm/s) [40]. Dingemans et al. have presented surface recombination velocities of <30 cm/s [5] whereas ~20 cm/s is shown by Gope et al. [25], both after annealing. Some discrepancies can be noticed in the charge values: in some cases as-deposited HfO_2 films have a positive charge [41] and in some cases it is negative [40, 42]. The postdeposition anneal affects the final charge value: it can change from negative to positive [42] or remain negative [40]. In contrast to that it has been shown that the charge in as-deposited HfO_2 is positive and depending on the film thickness it becomes negative after annealing [25]. Sreenivasan et al. demonstrate that the Hf precursor affects the fixed charge formation in HfO_2: using $HfCl_4$ leads to Cl rich interface and a negative fixed charge that is not affected even by high temperature anneals [43]. However, also positive fixed charges have been reported when $HfCl_4$ is used [25]. This indicates that the charge formation in HfO_2 does not depend only on the choice of Hf precursor but also other parameters related to ALD process might affect.

In this work, the effect of different ALD oxidants on the surface passivation quality of HfO_2 is studied. In the experiments, approximately 30 nm of HfO_2 was deposited on low resistivity (~3.5 Ωcm) n-type Cz-Si wafers by using TDMAH (tetrakis(dimethylamino)hafnium) as the Hf source. Three different oxidant variants were used to find the best process for surface passivation: i) H_2O, ii) O_3 and iii) H_2O+O_3. Low deposition temperature of 170°C in this study leads to amorphous film but during the postdeposition anneal at 450°C for 15 minutes the films will most likely crystallize [25]. Different oxidants for HfO_2 deposition have been studied also in various publications. Less hydrogen impurities have been measured in the O_3 based HfO_2 similarly as in Al_2O_3 [44]. The O_3 process is shown to have more N impurities and low amount of C impurities whereas in the H_2O process only C impurities are measured [45]. The existence of N impurities can lead to complex changes in the HfO_2 film during postdeposition heat treatments and hence affect the final surface passivation quality.

Figure 4a shows the injection level dependent lifetimes of the three different processes after postdeposition annealing measured with QSSPC. In the as-deposited state HfO_2 does not provide notable surface passivation and hence these values are not shown here. Both the O_3 and H_2O+O_3 processes provide relatively good surface passivation with

$S_{eff,max}$ values of ~30 cm/s and ~38 cm/s, respectively, at an injection level of 1×10^{15} cm^{-3}. The best surface passivation is reached with the pure H_2O process resulting in $S_{eff,max}$ = 14 cm^{-3} which is one of the lowest surface recombination velocities reported so far. The D_{it} and Q_{tot} values are presented in Figure 4b. The low D_{it} in the H_2O based sample is consistent with Al_2O_3 passivation studies: it is most likely caused by higher amount of hydrogen in the film deposited with H_2O and during annealing it diffuses into the interface passivating the interface defects. This could also explain the difference between the pure O_3 and H_2O+O_3 processes where slightly lower D_{it} value is observed with the combined process.

COCOS measurements show that regardless of the oxidant HfO_2 has a negative charge both in the as-deposited state and after annealing. After annealing, H_2O based processes have similar Q_{tot} values whereas in the pure O_3 process the charge is clearly higher (Figure 4b). This is also consistent with studies regarding Al_2O_3 passivation using different oxidants [21]. Overall, the charge values in the annealed HfO_2 samples are in the range of $(5\text{-}10)\times10^{11}$ cm^{-2} and hence slightly lower than the fixed charge in Al_2O_3. The best surface passivation with pure H_2O process can be explained with the lowest D_{it} value. Q_{tot} in the H_2O based processes is not as high as in the pure O_3 process where the lifetime is most likely deteriorated by the higher D_{it}. In the combined process the charge is in the same level as in the pure H_2O process but the higher D_{it} value lowers the lifetime.

More profound analysis of the film and interface properties is needed to fully explain the differences in the D_{it} and Q_{tot} values between these processes. These include chemical analysis to reveal *e.g.* the C, N and H impurity concentrations before and after annealing as well as high-resolution imaging to analyze the interfacial layer that can consist of SiO_x, hafnium silicate or SiO_x-rich hafnium silicate [46-47]. In conclusion, the results presented here verify that HfO_2 is a promising material for silicon surface passivation. It has also potential for n+ surface passivation for its fixed charge is slightly lower than in Al_2O_3 but the interface quality is excellent. HfO_2 could also provide better antireflection properties as compared to Al_2O_3.

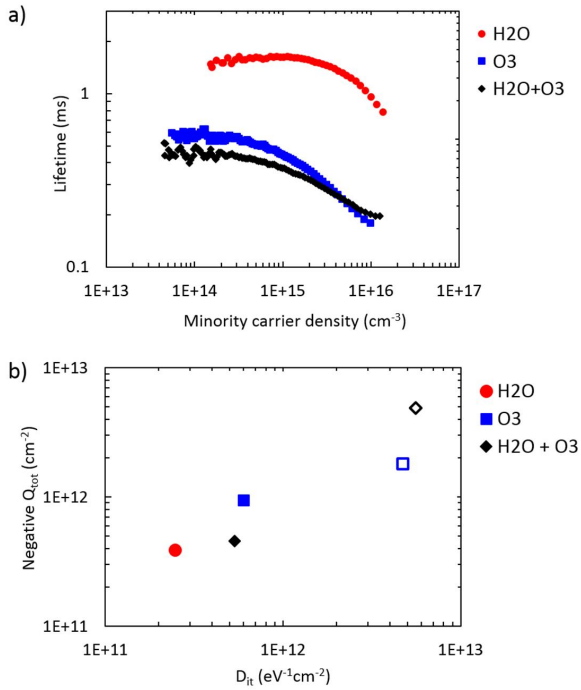

Figure 4. *a) Injection level dependent minority carrier lifetime of HfO_2 samples after annealing at 450°C for 15 minutes. Three different oxidants were used in the ALD process: i) H_2O, ii) O_3 and iii) H_2O+O_3. The ALD temperature was ~170°C. b) Negative total charge and the interface defect density of HfO_2 samples before (open symbols) and after (solid symbols) annealing. As-deposited data from H_2O sample is not available.*

.

3. Black silicon

3.1 Properties and fabrication

Black silicon (b-Si) has been a subject of great interest in various fields including photovoltaics [41-54] for its extremely low reflectance on a wide spectral range and acceptance angle (see Figure 5a). In practice, black silicon refers to a nanostructured surface with features smaller than the wavelength of light as presented in the scanning electron microscope (SEM) image in Figure 5b. The reason for the extremely low reflectance and hence black appearance is the refractive index gradient and so called "moth-eye" principle: silicon nanostructure forms a medium with *e.g.* air where the ratio of air and silicon varies gradually and hence no clear interface for light exists [55]. This naturally suppresses the Fresnel reflection quite efficiently. More thorough investigation regarding the optical properties of black silicon have shown that b-Si also scatters light leading to light trapping [56]. Otto et al. have compared different types of b-Si structures with varying profile depths and concluded that finding a perfect balance between light trapping and antireflection (*i.e.* moth-eye phenomena) is challenging: the best structure for light trapping might not be the best for antireflection and vice versa [57].

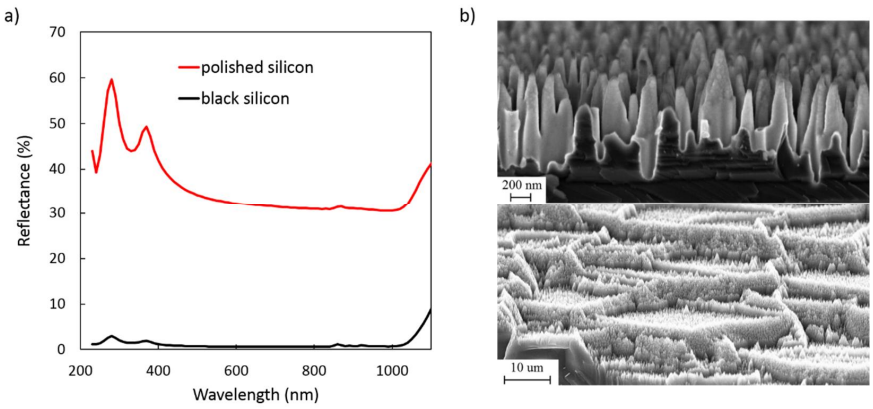

Figure 5. *a) Reflectance of b-Si surface as compared to polished silicon surface. Both surfaces have 20 nm Al_2O_3 coating on them. b) SEM image of black silicon structure on monocrystalline (above) and multicrystalline (below) silicon.*

Most common ways for black silicon fabrication are different types of etching methods including *e.g.* deep reactive ion etching (DRIE) [49], metal-assisted chemical etching (MACE) [58], laser etching [59], photoelectrochemical etching (PEC) [60] and plasma immersion ion implantation (PIII) [61]. Good descriptions of these methods are found in recent black silicon reviews by Liu et. al. [62], Otto et al. [57] and Hsu et al. [63]. In this thesis the focus is on cryogenic DRIE etching as it was used for b-Si formation in Publications III-VII. Black silicon fabrication with DRIE was originally used for process optimization and black silicon as the outcome was considered undesirable [64]. Etching b-

Si with DRIE has certain advantages: it is fast compared to laser etching and nanostructures can be made on one wafer surface without mask layers [49]. Additionally, unlike wet etching approaches, in DRIE the etch rate is independent of crystalline planes. In MACE problems arise from difficulties in removing metal contaminants which is not a problem in DRIE and unlike laser texturing it does not cause serious etching damage [65].

The cryogenic DRIE process used in this thesis employs a mixture of SF_6 and O_2 gases at a temperature of -120°C as presented in Figure 6. Plasma discharge is used to create F* radicals as well as positive and negative ions (SF_5^+, F^-) from SF_6 and O* radicals from O_2 gas, respectively. These reactive species are then directed from the plasma to the silicon surface where F* radicals absorb in it creating mainly volatile SiF_4. The reaction rate between silicon and fluorine is further increased by ion bombardment. Simultaneously, O* radicals react with SiF_4 creating silicon-oxyfluoride (SiO_xF_y) which acts as a passivating layer (*i.e.* hinders the reaction of Si and F*). Ion bombardment removes the passivating layer from horizontal surfaces but not from the vertical ones. This is what enables etching *e.g.* deep trenches with vertical sidewalls. For black silicon etching the process is slightly different: the amount of O_2 is increased which leads to thicker passivation layers that cannot be removed efficiently enough to create vertical sidewalls but sidewalls with positive slopes. This so called overpassivation is the key element in the b-Si formation.

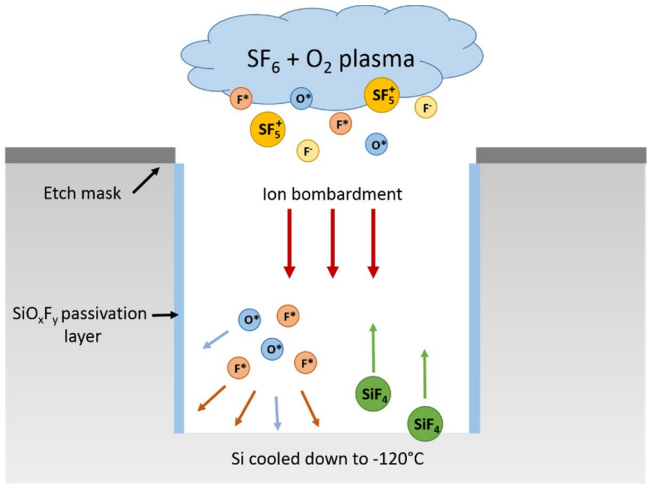

Figure 6. *The operation principle of cryogenic DRIE process. Fluorine and oxygen radicals as well as different types of ions are created in the $SF_6 + O_2$ plasma. Fluorine radicals react with silicon resulting mainly in volatile SiF_4 species. Also other species such as SiF_2 can be produced but in much lower proportion. Oxygen radicals react with SiF_4 creating SiO_xF_y passivation layer that is removed from horizontal surfaces by ion bombardment while vertical sidewalls remain passivated.*

Although the process described above is well known, one fundamental question remains open: what actually initiates black silicon formation? It is proposed that behind the formation is micromasking [66] or trenching *i.e.* the etch pitches grow as the etching

proceeds and finally unite forming spikes [67]. However, as discussed by Dussart et al. [68] micromasking cannot be the main mechanism behind black silicon formation due to the relatively organized structure. This indicates rather that the initial surface roughening due to competing etching and passivating reactions could help initialize the structure formation [69].

3.2 Surface passivation

Many black silicon applications - particularly solar cells - suffer from increased surface recombination resulting in poor spectral response especially at short wavelengths. This effect is often more detrimental for the final device operation than the gain from the reduced reflectance. For surface passivation of black silicon both thermal SiO_2 [53] and PECVD SiN_x [70] have been used with varying results. It has been shown *e.g.* that the conformality of PECVD SiN_x is poor on nanostructured surfaces [10] which can partly explain the moderate efficiencies reached with black silicon solar cells.

The potential of ALD Al_2O_3 to solve the surface passivation issue of b-Si is addressed in Publication III. Although the combined process of O_3 and H_2O have provided better surface passivation on planar samples as described above (Publication I), O_3 was chosen as the oxidant for the b-Si study since there is no blistering in Al_2O_3 deposited with pure O_3. The conformality and especially the high total negative charge of Al_2O_3 [65] lead to millisecond lifetimes on low resistivity Cz material corresponding to surface recombination velocity of ~22 cm/s (see Figure 7a). No sufficient surface passivation is gained in the reference samples with thermal SiO_2 passivation. Figure 7b shows the minority carrier lifetimes as a function of injection level in two sister mc-Si wafers coated with Al_2O_3, both with and without b-Si surface. There is no significant difference between the samples in lifetime which indicates that Al_2O_3 can also passivate multicrystalline b-Si surfaces. Lifetimes nearly 200 μs were reached in both cases when measured from corresponding good quality grains. Calibrated photoluminescence (PL) lifetime mapping and quasi-steady state photoluminescence (QSSPL) [71] measurements were done for the mc-Si samples to omit the trapping effect and the uncertainty of the optical constant in QSSPC.

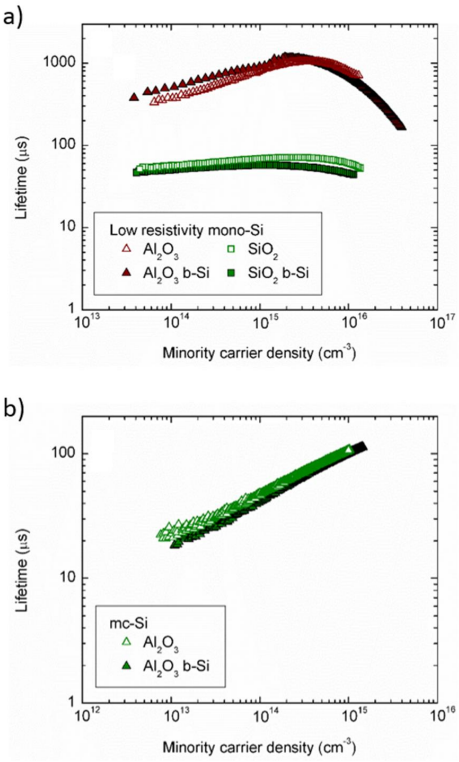

Figure 7. *Minority carrier lifetimes as a function of injection level of a) the low resistivity Cz samples and b) mc-Si samples. Cz samples were measured with QSSPC and mc-Si with QSSPL. For Cz-Si, four types of samples were processed: b-Si surfaces with Al_2O_3 and SiO_2 and, as a reference, similar samples but with polished surfaces. For mc-Si, two types of samples were prepared: Al_2O_3 coated mc-Si wafers with and without b-Si. (Reprinted with permission from P. Repo, A. Haarahiltunen, L. Sainiemi, M. Yli-Koski, H. Talvitie, M. C. Schubert and H. Savin, Journal of Photovoltaics 3, 90-94 (2013). Copyright 2013, IEEE)*

Reflectance values of approximately 1% and below are reached in Al_2O_3 coated b-Si samples indicating that besides reducing the surface recombination the coating further suppresses also the reflectance as presented in Figure 8a. The small difference in reflectance between the SiO_2 and Al_2O_3 coated samples can be attributed partly to the changes in the nanostructures caused by the thermal oxidation whereas the thin and conformal ALD layer maintains the antireflection properties of the nanostructures. The differences in the refractive indices of SiO_2 and Al_2O_3 can also have some effect. The lowest reflectance value of all samples, less than 0.85% in the whole wavelength range, is measured from the b-Si etched mc-Si sample coated with Al_2O_3 (Figure 8b). This can be explained by the multi-scale texture caused by the combination of the initial surface roughness of mc-Si and the b-Si etching (see Figure 5b).

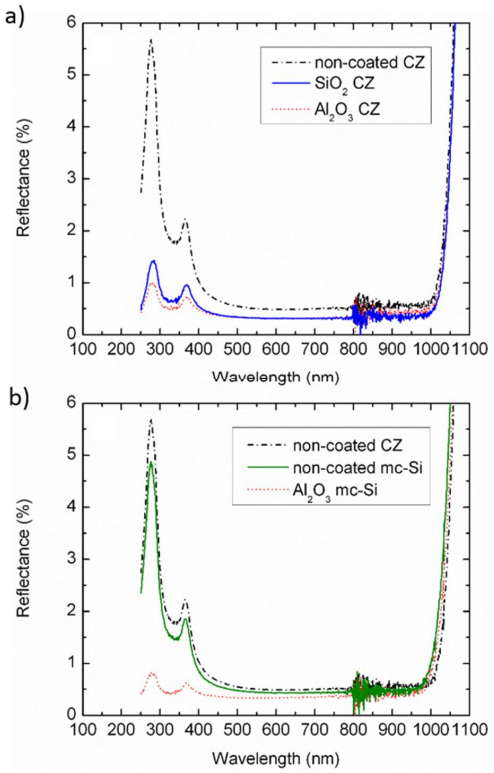

Figure 8. *Reflectance of a) monocrystalline silicon with non-coated, SiO_2 coated and Al_2O_3 coated b-Si surfaces and b) mc-Si with either non-coated and Al_2O_3 coated b-Si surfaces. Also the reflectance of the non-coated low resistivity Cz sample is included in b) for comparison. (Reprinted with permission from P. Repo, A. Haarahiltunen, L. Sainiemi, M. Yli-Koski, H. Talvitie, M. C. Schubert and H. Savin, Journal of Photovoltaics 3, 90-94 (2013). Copyright 2013, IEEE)*

In summary, the results presented above prove that ALD Al_2O_3 has a potential for being a material that effectively lowers the reflectivity and passivates black silicon surfaces that have less than 1% reflectance. The results were obtained in summer of 2011, which was the first successful demonstration of b-Si surface passivation with ALD Al_2O_3. Consequently, invention disclosure at Aalto University was made and the results were first presented in SiliconPV conference in spring 2012 [72]. Later on, ALD surface passivation of b-Si has raised interest also among other research groups. For instance, similar surface passivation of b-Si with ALD Al_2O_3 has also been demonstrated by Otto et al. by using H_2O as the oxidant [73].

3.3 Role of different oxidants

Recent studies have shown that using ozone as an oxidant in Al_2O_3 deposition leads to enhancement in the surface passivation and especially in the field effect due to higher negative oxide charge [21]. Therefore, it could be expected that higher negative charge is

beneficial also for the passivation of b-Si surfaces where the effect of charge is more pronounced [65]. Evidently, good surface passivation was reached with the O_3 process on b-Si as presented previously (Publication III). However, in Publication I using O_3 as the oxidant led to lower lifetimes than using the combined process of H_2O and O_3 in planar wafers. As there are clear differences in the passivation of planar surfaces when different oxidants are used there might also be some on b-Si. Hence, the effect of using different oxidants in ALD Al_2O_3 passivation on b-Si surfaces is further studied in Publication IV.

Three different processes were chosen to study the effect of the oxidants. TMA was used as the aluminum source in all the processes but the oxidant was varied similarly as in the case of HfO_2: i) H_2O, ii) O_3 and iii) H_2O+O_3. Approximately 25 nm of Al_2O_3 was deposited on both sides of each p-type magnetic Cz-Si wafer (~3 Ωcm) at 200°C. Both b-Si and planar reference wafers were processed. Passivation was activated by annealing at 400-430°C for 30 minutes in nitrogen atmosphere. Further optimization as compared to the processes used in Publication I and III was carried out *i.e.* the precursor pulse times were increased to guarantee that saturation is reached also on the large surface area of black silicon. The reactor configuration was also different between these experiments: smaller reactor with more optimal flow was used in later experiments.

Figure 9 shows the injection level dependent minority carrier lifetime for both black silicon and their planar counterparts after three different ALD processes and postdeposition anneal. With processes using O_3 as the oxidant (O_3 or H_2+O_3) lifetime in planar wafers is higher than in the corresponding b-Si samples. This is not surprising taking into account the larger surface area of b-Si. These processes provide surface recombination velocity of ~12 cm/s on planar and ~22-24 cm/s on black silicon. In the process where pure H_2O is used the result is opposite: lifetime in b-Si sample is a bit higher than in the corresponding planar reference having surface recombination velocities of ~21 cm/s and 43 cm/s, respectively. The difference could be explained at least partly by blistering: severe blistering is observed in the planar H_2O sample whereas in b-Si it was not observed. Surprisingly, the lifetime in the H_2O b-Si sample is higher than in the b-Si samples where O_3 is used, especially in the case of pure O_3. This is unexpected because higher Q_{tot} values have been reported for O_3 processes which should be even more beneficial for b-Si surface passivation.

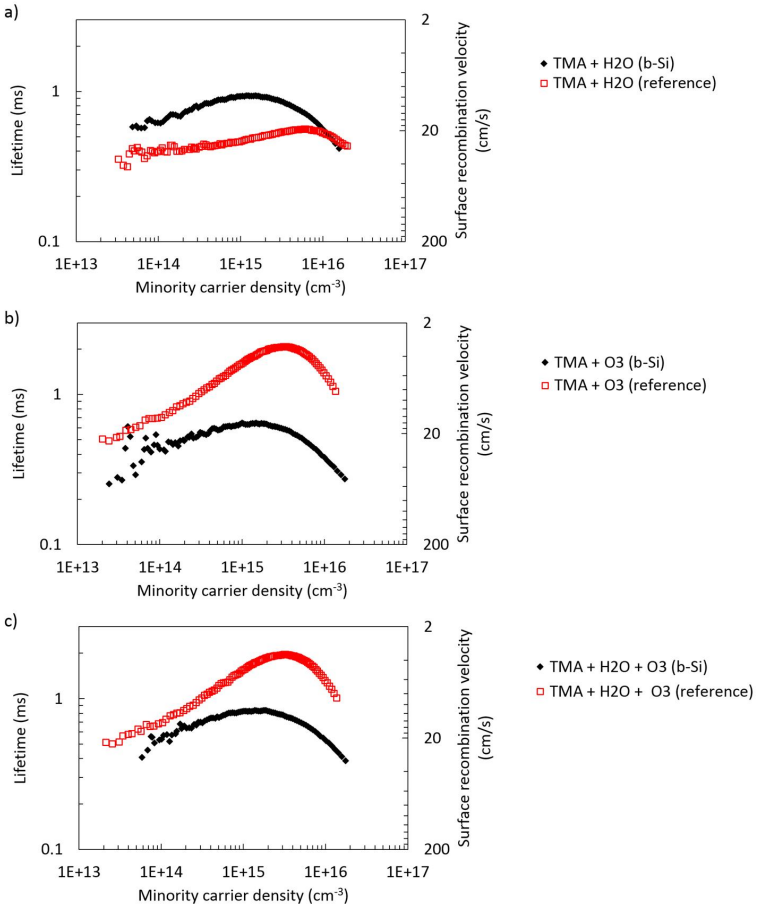

Figure 9. *Injection level dependent carrier lifetime and surface recombination velocity of both black silicon and planar counterparts after three different ALD processes: i) TMA+H_2O, ii) TMA+O_3 and iii) TMA+H_2O+O_3. Samples were measured with QSSPC after annealing at 400-430°C for 30 minutes. (Reprinted with permission from P. Repo and H. Savin. Copyright 2016, Elsevier Ltd.)*

To investigate the reason why H_2O processes provide better passivation for b-Si than pure O_3 process, COCOS measurements were performed both on planar and b-Si samples. H_2O samples show lowest Q_{tot} value (see Figure 10a) while the value is the highest when pure O_3 is used, which is in agreement with literature [21, 74]. This applies both for planar and b-Si samples. According to previous results [65], the measured charge in b-Si is effective and could be scaled to a local value that corresponds the one measured from planar wafers. This is done by dividing the charge by the increase in surface area. In our case the charge in b-Si samples is approximately three times higher than in the planar references which corresponds quite well the area enhancement of the black silicon structure in these samples.

Midgap D_{it} values measured from planar reference wafers are presented in Figure 10b. The D_{it} value is slightly higher in the ozone process than in the H_2O-based processes.

This is in agreement with previously published results and may be related to the higher interface carbon density and lower interface hydrogen density in the pure O_3 process at this O_3 concentration [21]. The D_{it} values measured from b-Si have a similar trend as the planar counterparts. However, the interpretation of D_{it} from COCOS measurements in the case of b-Si needs to be addressed further.

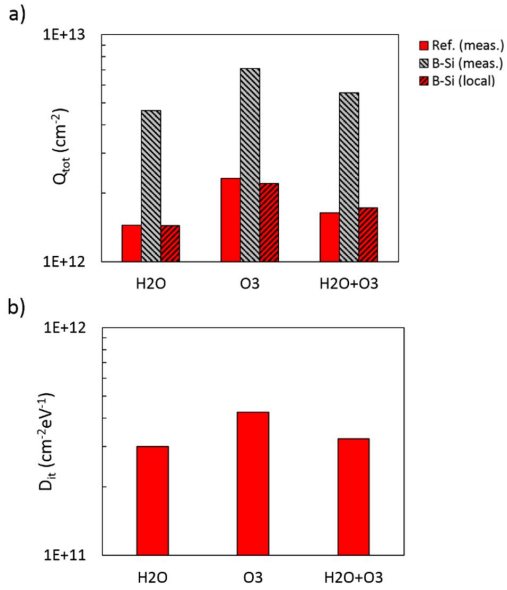

Figure 10. *a) Total fixed charge density and b) interface defect density after three different ALD processes. Local fixed charge values were rescaled by three from the measured values according to [65]. Samples were measured after annealing at 400-430°C for 30 minutes. (Reprinted with permission from P. Repo and H. Savin. Copyright 2016, Elsevier Ltd.)*

As b-Si enhances the effect of Q_{tot} it would be expected that O_3 process leads to best passivation in the case of b-Si. However, the behavior seems to be opposite. Possible differences *e.g.* in the thickness and uniformity of the interfacial SiO_x layer caused by the use of different oxidants could help explaining why H_2O process is better for b-Si than pure O_3 process. Another reason for the differences could be that the O_3 process still needs further optimization as O_3 can decompose at temperatures >200°C. Not sufficient amount of O_3 could lead to non-uniformity of the film and hence poorer passivation. However, although the reason for the differences in b-Si passivation is not fully explained yet, relatively good surface passivation is reached with all oxidant combinations.

3.4 Emitter passivation

As surface passivation of b-Si with ALD Al_2O_3 has shown good results the next step towards actual solar cells is to study the passivation of emitters with the same method. There are two important questions that needs to be answered: i) Is the black silicon surface

passivation by ALD still efficient after emitter formation? ii) Does the dopant glass removal have an effect on the b-Si structure and the reflectance? In Publication V the emitter formation on b-Si and the subsequent surface passivation were studied. Two diffusion temperatures were chosen for double-sided BBr_3 tube furnace diffusion as summarized in Table I. N-type FZ-Si wafers with 5 Ωcm resistivity were used as the base material. On a planar surface, diffusion at 890°C or at 910°C for an hour should lead to emitters with a sheet resistance of ~90 Ω/sq and ~70 Ω/sq, respectively. In addition some of the samples went through a 1h drive-in oxidation at 1050°C after the diffusion at 890°C in order to lower the surface doping and have a deeper emitter profile. This should also be the process that affects most the b-Si structure due to additional oxidation. For surface passivation, 10 nm of Al_2O_3 was deposited on both wafer surfaces with plasma-assisted ALD (PA-ALD) at 180°C. Although this process was not tested before on black silicon it was the only one available without risking the samples during shipment to another facility. The process however had shown excellent passivation quality on planar and pyramid textured surfaces with boron emitters so the potential also for sufficient passivation on b-Si was evident [75, 76].

Table I. *The different processing sequences implemented to study emitter formation on black silicon and the surface passivation of b-Si emitters.*

Diffusion temperature & time	BSG etching	Drive-in oxidation	Passivation
890°C, 1 h	50 % HF	-	Al_2O_3
910°C, 1 h	50 % HF	-	Al_2O_3
890°C, 1 h	50 % HF	1050 °C	Al_2O_3

In Figure 11 the reflectance of b-Si surfaces after different diffusion processes as well as in the initial state, *i.e* directly after etching, is shown. Surprisingly, there are no significant changes in the reflectance even in the sample having combination of diffusion and a following drive-in oxidation. The small increase in the reflectance indicates that there can be some changes in the nanostructure. This can be verified by the SEM images in Figure 12 where the b-Si structure is shown before and after diffusion and drive-in. Indeed, small changes in the nanostructure height and shape can be seen, *i.e.* the needles become shorter and sharper. The fact that diffusion can be done without causing drastic changes in the reflectance gives more freedom also in the optimization of the emitter profile *i.e.* if a deeper emitter is needed a drive-in can be applied without losing the good optical properties of black silicon.

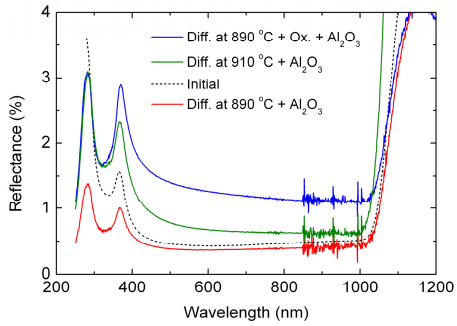

Figure 11. *Initial b-Si reflectance and the reflectances after different diffusion processes. 10 nm Al_2O_3 film was deposited on the diffused samples. (Reprinted with permission from P. Repo, J. Benick, G. von Gastrow, V. Vähänissi, F. D. Heinz, J. Schön, M. C. Schubert and H. Savin, Physica Status Solidi Rapid Research Letters 7, 950-954 (2013). Copyright 2013, Wiley-VCH Verlag GmbH & Co. KGaA)*

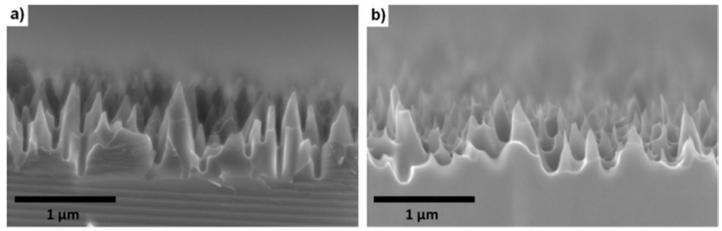

Figure 12. *SEM image from a black silicon surface a) before and b) after boron diffusion at 890°C and the subsequent drive-in oxidation. Boron glass was removed before the drive-in oxidation. (Reprinted with permission from P. Repo, J. Benick, G. von Gastrow, V. Vähänissi, F. D. Heinz, J. Schön, M. C. Schubert and H. Savin, Physica Status Solidi Rapid Research Letters 7, 950-954 (2013). Copyright 2013, Wiley-VCH Verlag GmbH & Co. KGaA)*

Simulations with Sentaurus Process [77] indicate that all diffusion processes used in this study lead to a complete doping of the nanostructure *i.e.* the junction is nearly flat under the surface and only mildly follows the surface structure as presented in Figure 13. The consumption of silicon during boron glass formation and drive-in oxidation was taken into account in the simulations [78]. The deepest emitter profile is reached in the process with drive-in oxidation whereas only a small difference in the junction depth between diffusion temperatures of 890°C and 910°C is seen. Changes in the b-Si structure are also as expected: the most prominent change is seen when the drive-in oxidation is performed while a small change in the diffusion temperature has only a minor effect on the structure.

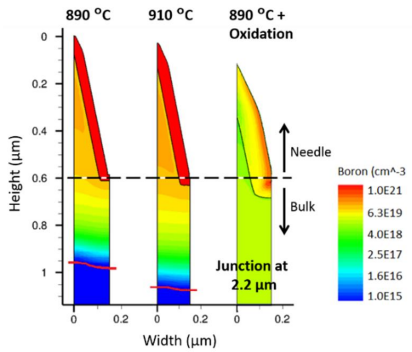

Figure 13. *Diffusion simulation results using a symmetry element with the height of 0.6 µm and width of 0.15 µm. The red coating on the two leftmost symmetry elements depict the boron glass that was removed before drive-in oxidation. In the symmetry element on the right the utmost layer is the oxide formed during the drive-in oxidation.*

Figure 14 shows the measured inverse effective lifetime and the corresponding emitter saturation current density J_{0e} of the most industrially relevant b-Si sample, *i.e.* after diffusion at 910°C. J_{0e} value of 51 fA/cm^2 prove that an efficient surface passivation can be obtained with an industrial type of emitter. As a reference, J_{0e} values as low as ~11 fA/cm^2 have been reached on high efficiency boron emitters and 20-25 fA/cm^2 on more industrial type emitters with Al_2O_3 passivation [76]. These results are for planar surfaces and naturally for textured surfaces the values are higher: for industrial type emitters with random pyramids J_{0e} values of ~45 fA/cm^2 are reached when using Al_2O_3/SiN_x stacks for surface passivation [79]. Calculated $V_{oc,max}$ value of 703 mV (T = 25 °C, J_{sc} = 40 mA/cm^2) proves that black silicon with Al_2O_3 surface passivation could be applied on high-efficiency n-type solar cells. The effective lifetime τ_{eff} at an injection level of 1×10^{15} cm^{-3} was 0.78 ms and the implied open-circuit voltage $V_{oc,impl}$ = 688 mV (at 1 sun), both measured with QSSPC.

In conclusion, Al_2O_3 provides efficient surface passivation on nanostructured boron doped emitters, which is the first step towards high efficiency n-type black silicon solar cells. With an emitter saturation current density of 51 fA/cm^2 open-circuit voltages of around 700 mV are achievable. The effect of different diffusion processes on the optical properties of low-reflectivity black silicon is small although there is a change in the nanostructure: extremely low average reflectance values – even as low as 0.5 % – can still be reached after depositing a thin layer of Al_2O_3. These results show that diffusion can be applied on a black silicon surface without losing the good optical properties and prove the potential of using black silicon as the front surface texture on high-efficient n-type solar cells.

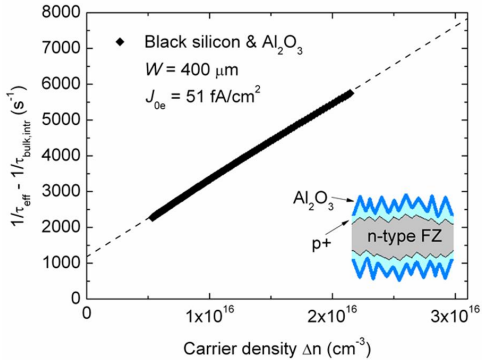

Figure 14. *Inverse effective lifetime corrected with the intrinsic bulk lifetime as a function of injection level. The corresponding linear fit is shown with a dashed line and the inset presents a schematic of the J_{0e} sample. For surface passivation 10 nm of Al_2O_3 was deposited on both wafer surfaces with PA-ALD at 180°C. The passivation was activated with a forming gas anneal (FGA) at 425 °C for 25 minutes. (Reprinted with permission from P. Repo, J. Benick, G. von Gastrow, V. Vähänissi, F. D. Heinz, J. Schön, M. C. Schubert and H. Savin, Physica Status Solidi Rapid Research Letters 7, 950-954 (2013). Copyright 2013, Wiley-VCH Verlag GmbH & Co. KGaA)*

4. Black silicon devices

Since excellent results regarding surface passivation of b-Si both on lowly and highly doped surfaces are reached the next logical step is to demonstrate its benefit on device level. So far, black silicon solar cells have shown only moderate efficiencies of ~18% or less with both SiN_x and SiO_2 surface passivation [51, 53, 70]. The best front-contact solar cell with b-Si was reported by Oh et al. with the efficiency of 18.2% [80]. In the next chapters the improvement in performance on different types of devices is presented as b-Si with Al_2O_3 passivation is integrated into them.

4.1 Front contact solar cells

In Publication VI, PERL (passivated emitter with rear locally diffused) solar cells with black silicon on the front surface were fabricated on n-type 5 Ωcm FZ-Si (400 µm) wafers. The solar cell structure is shown in Figure 15. Reference cells with inverted pyramids and an Al_2O_3/SiN_x stack on the front surface were processed alongside with the black silicon cells featuring only Al_2O_3 at the front. The only difference in the reference cell process was the front surface texturization and the deposition of 65 nm of SiN_x with PECVD. Emitter formation corresponded the ones presented in Chapter 3.4. (Publication V) except the process with drive-in oxidation was omitted and a third diffusion temperature of 930°C was introduced. For the front surface passivation 10 nm of Al_2O_3 was deposited with PA-ALD whereas for the rear surface passivation the *PassDop* [81] process was applied.

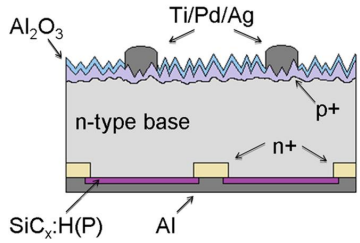

Figure 15. *Schematic of the applied solar cell structure. PassDop was applied as the rear surface passivation material. It consists of hydrogenated silicon carbide doped with phosphorous. When the contact openings are done through the PassDop layer with a laser, phosphorus creates local back surface fields to ensure better contacts on the rear surface. (Reprinted with permission from P. Repo, J. Benick, V. Vähänissi, J. Schön, G. von Gastrow, B. Steinhauser, M. C. Schubert, M. Hermle and H. Savin, Energy Procedia 38, 866-871 (2013). Copyright 2013, The Authors, Published by Elsevier Ltd.)*

The solar cell parameters measured at 1 sun as well as the pseudo fill factors (PFF) are shown in Table II. All cells, including the reference cell, exhibit a relatively low open-circuit voltage of ~630 mV. The comparison with the internal quantum efficiency (IQE) reveals that all cells suffer from an insufficient rear side passivation. This is mainly due to

the fact that the processing sequence was not adopted to meet the temperature requirements of both, the front side Al_2O_3 as well as the rear side *PassDop* layer, *i.e.* the high temperature applied for the annealing of the Al_2O_3 degraded the rear surface passivation. The front surface passivation, nevertheless is quite effective for all cells, as can be seen by the high IQE in the short wavelength range in Figure 16. This is coherent with the J_{0e} value of 51 fA/cm^2 discussed in Chapter 3.4. indicating an efficient surface passivation (Publication V). Nevertheless, the highest IQE is reached with the reference cells. For the b-Si cells the IQE reduces with increasing diffusion temperature. However, an adoption of the diffusion process might increase the IQE to the same level as the reference cells.

The reference cell with the inverted pyramids shows the highest short-circuit current of 39.9 mA/cm^2. The short-circuit current of the black silicon cells is slightly lower and shows a small dependence on the diffusion temperature: the higher the diffusion temperature *i.e.* the deeper and more highly doped the emitter, the smaller the short-circuit current density, as can be seen also in the IQE. Omitting the effect of the reflectance from the contacts the black silicon cells exhibit an average reflectance (R_w) of ~2-3 % which is higher than could be expected (see Figure 16). This naturally plays a role in the relatively low J_{sc} values. However, the reason for the higher reflectance values in b-Si was in one of the cleaning steps; the cleaning solution was unnecessary strong and it slightly etched the black silicon surface. This is easily avoided in future processing.

Table II. *The solar cell parameters from the three different black silicon cells and the reference cell with inverted pyramids measured at 1 sun. The pseudo fill factors (PFF) were measured with Suns-V_{oc}. Cell area was 4 cm^2.*

Surface structure	Diffusion T (°C)	J_{sc} (mA/cm^2)	V_{oc} (mV)	PFF (%)	FF (%)	η (%)
Black silicon	890	39.3	628	80.1	75.8	18.7
Black silicon	910	39.2	632	79.8	75.8	18.7
Black silicon	930	38.4	630	80.3	76.1	18.4
Inverted pyramids	910	39.9	631	77.2	75.3	18.9

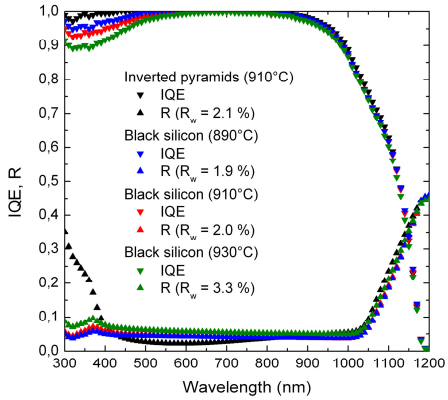

Figure 16. *The internal quantum efficiencies (IQE) and reflectances (R) of the different black silicon cells and the reference cell with inverted pyramids and an Al_2O_3/SiN_x stack. Spectrum weighted average reflectances (R_w) were calculated by taking into account only the front surface reflection although the escape is still shown in the figure. The reflection from the contacts was also omitted in the R_w calculation. (Reprinted with permission from P. Repo, J. Benick, V. Vähänissi, J. Schön, G. von Gastrow, B. Steinhauser, M. C. Schubert, M. Hermle and H. Savin, Energy Procedia 38, 866-871 (2013). Copyright 2013, The Authors, Published by Elsevier Ltd.)*

The fill factor of all cells is relatively low and the root cause of this needs to be further investigated. SEM image in Figure 17 shows a cross section of the b-Si surface under the evaporated metal contact. As can be seen the metal does not reach the extremely small gaps on the b-Si surface which might lead to an increased series resistance. However, also the reference cells suffer from a low FF. This can be related to the used base material with relatively high resistivity but more experiments are needed to have a more thorough analysis. The pseudo fill factor values are also lower than expected indicating that the low FF values cannot be completely explained by a high series resistance. No shunting could be observed based on the *I-V* characteristics.

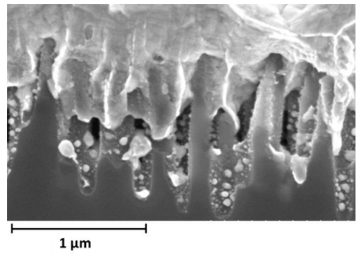

Figure 17. *An SEM image of the black silicon and front metal contact interface showing how the metal is mostly deposited on the nanostructure and does not reach the valleys of the structure. (Reprinted with permission from P. Repo, J. Benick, V. Vähänissi, J. Schön, G. von Gastrow, B. Steinhauser, M. C. Schubert, M. Hermle and H. Savin, Energy Procedia 38, 866-871 (2013). Copyright 2013, The Authors, Published by Elsevier Ltd.)*

In total, a cell efficiency of 18.7% could be reached for these very first n-type b-Si cells with Al_2O_3 surface passivation. This proves that b-Si is a promising approach for the

front side texturing. Most importantly it is demonstrated that the nanostructured front surface is not destroyed during the multiple processing steps including diffusion, boron glass etching as well as resist application and stripping needed in lithography. In order to optimize the emitter diffusion process for a black silicon surface it is important to gain more information about the emitter profile. This has already been and will further be addressed with process simulations whereas measuring the profile might be possible *e.g.* with electrochemical capacitance voltage (ECV) method. Optimizing the emitter profile relates to the optimization of the surface passivation and the metallization from which especially the metallization should be further addressed. The annealing treatments required by the Al_2O_3 and the *PassDop* passivation should also be fitted to the process accordingly. With more process optimization considerably higher efficiencies can be expected.

4.2 Back contact solar cells

As discussed in the previous chapter, some optimization is needed to fully utilize black silicon in conventional front contact solar cells. Among these are the considerations regarding good metal contact on b-Si and optimized emitter diffusion. Although it is likely that these issues can be solved with further process optimization they can be also avoided completely. The solution for this are interdigitated back contact (IBC) solar cells where the junction and the contacts are placed at the back of the cell and hence both Auger recombination in the highly doped nanostructures [80] as well as the problems with the contact formation are no longer an issue. Figure 18 shows the cross-section of the IBC cell structure with b-Si front surface texture introduced in Publication VII. The collecting junction is on the back side, and no contacts (and thus no shadowing) are present on the front side. The cells introduce selective emitters, meaning that there is a heavily doped region just beneath the contact to reduce the contact resistance and to hide the highly recombining contact from the rest of the junction. Four different emitter coverages were applied: 67, 75, 80 and 86%. P-type FZ-Si wafers with a resistivity of 2.6 Ωcm and thickness of 280 μm were used as the base material.

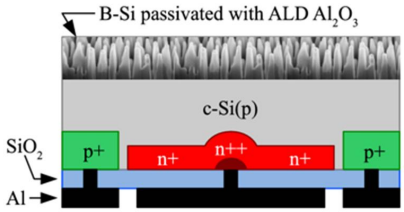

Figure 18. *Structure of the IBC solar cell. A thin Al_2O_3 layer was deposited on the nanostructured front surface. On the back surface green represents the boron and red the phosphorus diffusions respectively. SiO_2 was used for rear surface passivation and Al as contact material. Identical solar cells, but with a random pyramid texture, were fabricated as a reference. The surface area of the cells was 9 cm^2. (Reprinted with the permission from H. Savin, P. Repo, G. von Gastrow, P. Ortega, E. Calle, M. Garín, and R. Alcubilla, Nature Nanotechnology 10, 624-628 (2015). Copyright 2015, Macmillan Publishers Limited.)*

The current-voltage (*J-V*) and power-voltage (*P-V*) characteristics of the best b-Si solar cell are shown in Figure 19a. These results were obtained for an emitter coverage of 80%. The photovoltaic parameter values are summarized in Table III, where the results are directly compared with the reference counterpart (cell with random pyramid texture). Measurements from the b-Si solar cell show efficiencies over 22.1% (independently confirmed at Fraunhofer ISE CalLab PV Cells testing laboratory) which equals the efficiency of the reference counterpart. The high short-circuit current density J_{sc} of 42.2 mA/cm^2, as well as the good open-circuit voltage V_{oc} of 665 mV, prove the excellent front-surface passivation in the b-Si cell. This is also clearly seen from the external quantum efficiency (EQE) measurements in Figure 19b, which show a flat behavior in the short wavelength range with a value around 96%. In fact, the main difference with the reference counterpart cell is in the short wavelength range, where the reference cell clearly exhibits lower EQE values. This can be attributed to the much lower reflectance of the b-Si in the ultraviolet range. The similar EQE values in the infrared region (λ = 800–1200 nm) indicate near identical rear surfaces on both the b-Si and reference cells, as can be expected.

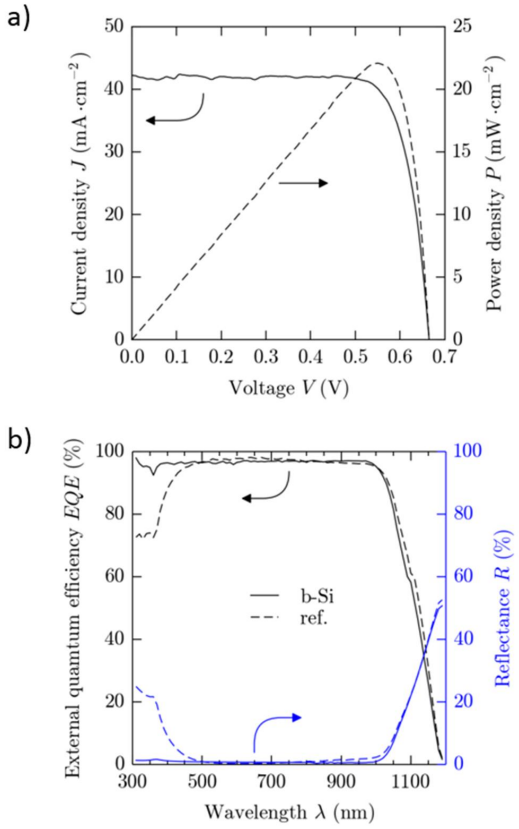

Figure 19. *a) J-V and P-V characteristics of the b-Si cell with 80% emitter coverage and b) EQE and reflectance measurements for the best b-Si and the corresponding randomly texturized cell. EQE's were measured with 0.1 suns bias light. (Reprinted with the permission from H. Savin, P. Repo, G. von Gastrow, P. Ortega, E. Calle, M. Garín, and R. Alcubilla, Nature Nanotechnology 10, 624-628 (2015). Copyright 2015, Macmillan Publishers Limited.)*

Table III. *The solar cell parameters for the b-Si and corresponding reference solar cell with emitter coverage of 80%.*

Surface structure	J_{sc} (mA/cm^2)	V_{oc} (mV)	FF (%)	η (%)
Black silicon	42.2	665	78.7	22.1
Random pyramids	42.0	667	78.6	22.0

Due to the b-Si property of absorbing light with high acceptance angles, the high efficiency can be maintained independently of the direction of the incoming light (Figure 20a). This is not the case with conventional AR coatings, which are only optimized for incident light perpendicular to the cell surface. This property has a high impact, especially in photovoltaics, because the Sun's radiation impinges solar cells from different angles throughout the day and through the year. Figure 20b shows the relative change in the photogenerated current with respect to normal illumination, for several incidence angles

and considering both the reference and b-Si cells. For the b-Si cell, changes in the photogenerated current are under 1% for incidence angles below approximately 60°, whereas the reference counterpart loses up to nearly 4% in the same angle range. As a consequence, the quantity of energy delivered by the b-Si cell throughout the day/year also surpasses the energy produced by the reference solar cell. For latitudes below 60° (Helsinki), relative increases greater than 2% are obtained over the year. This improvement is dependent on season. For instance, far from the equator, the increase is more important when insolation is lower (winter) and this asymmetry grows with latitude. As can be seen in Figure 20c, at 40° of latitude the increase is more than 2.5% during the four months with less insolation.

These results indicate that b-Si is not limiting the cell efficiency, so further improvements should be possible by improving the cell structure. Since Al_2O_3 passivation has been reported to work on n-type surfaces as well [14], also n-type IBC cells have been fabricated in order to benefit from the higher bulk minority carrier lifetimes [82]. Furthermore, even higher efficiencies could be expected by optimizing the emitter coverage. Other improvements could be implemented in current IBC structures to increase FF and V_{oc} values. For instance, a thicker aluminum layer in fingers and busbars would reduce ohmic losses, thereby achieving higher FF values. Moreover, an optimized phosphorous doping profile in the low and high doped emitter regions might further decrease the emitter saturation current density increasing V_{oc} accordingly. Therefore, with realistic improved values of FF > 81% and V_{oc} > 675 mV, and assuming the excellent J_{sc} (42.2 mA/cm^2) value, efficiencies well beyond 23% are reachable. One further possibility is to apply ALD AlN for the rear surface passivation. As discussed in Chapter 2.3. AlN provides good chemical passivation and has a moderate charge and hence it could provide better surface passivation for both n+ and p+ as compared to thermal SiO_2 used now at the back surface of the cell.

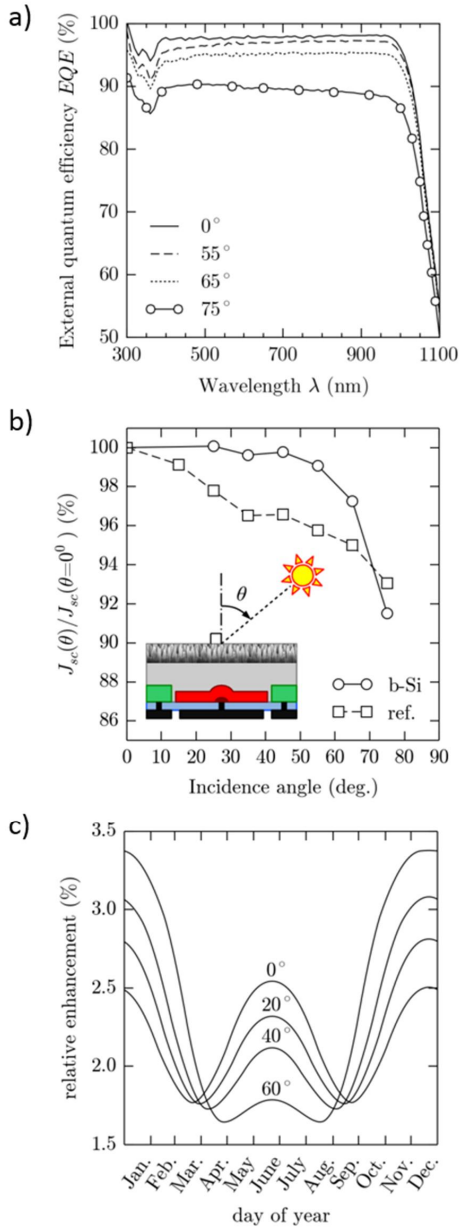

Figure 20. *a) Measured EQE of the b-Si cell for different angles of incidence, b) relative photocurrent, with respect to photocurrent at normal incidence, for different light incidence angles for both the black silicon and the reference solar cells and c) calculated daily relative increase along the year of the energy generated by the black silicon cell compared to the reference cell for different locations (60° latitude corresponds to Helsinki, 40° to Barcelona). (Reprinted with the permission from H. Savin, P. Repo, G. von Gastrow, P. Ortega, E. Calle, M. Garín, and R. Alcubilla, Nature Nanotechnology 10, 624-628 (2015). Copyright 2015, Macmillan Publishers Limited.)*

4.3 Induced junction photodiodes

The potential of black silicon is not limited only to solar cells. Any other component that requires a large surface area or extremely low reflectance is a potential application. These include *e.g.* microelectromechanical systems (MEMS) [83], ion mobility spectrometers (IMS) [84], terahertz emitters [85], drug analysis [86], and photodetectors [87]. Here, a black silicon photodiode where Al_2O_3 surface passivation is applied to ensure better charge collection probability is introduced. In addition to surface passivation the negative charge in Al_2O_3 is used to create the collecting junction via inversion on the front surface of a high resistivity (>10 kΩcm) n-type FZ-Si wafer as presented in Figure 21. Similar devices have been realized before on p-type wafers with thermal SiO_2 [88]. The role of b-Si is also twofold: black silicon enhances the field-effect that creates the inversion layer and the low reflectance ensures that smaller amounts of light entering also from wider angles can be detected.

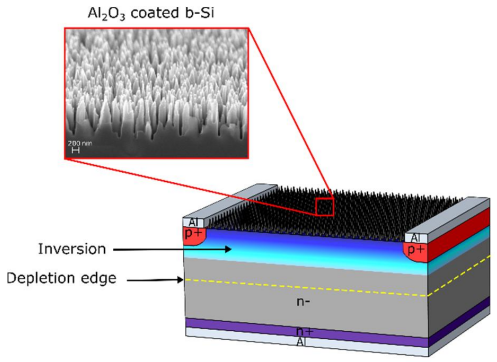

Figure 21. *Cross section of the photodiode concept. Surface of high resistivity (>10 kΩcm) n-type silicon is covered with Al_2O_3 coated black silicon. Charge in Al_2O_3 induces an inversion layer on the silicon surface which leads to formation of depletion region. Inversion is contacted with aluminum on top of p+ doped ring and the bulk is contacted with aluminum on top of n+ doped layer on the back side. The device area is 5x5 mm^2.*

The existence of an inversion layer was confirmed by standard current voltage (*I-V*) measurements that showed conventional diode characteristics. To get deeper insight on the properties of the collecting junction device simulations were performed with Silvaco Atlas. Down to the depth of approximately 9 µm from the device front surface the hole concentration exceeds the electron concentration, indicating inversion. The associated depletion region edge extends down to approximately 30 µm of depth, which suggests that the collection efficiency should be comparable to that of a conventional pn-junction.

Figure 22 shows both the spectral response and the external quantum efficiency of the b-Si photodiode. The dashed line in Figure 22 indicates the response and EQE of an ideal photodiode corresponding to exactly one charge carrier collected for each photon arriving at the surface. As can be seen, the b-Si photodiode has a very high and extremely

uniform response, following the 100% quantum efficiency line. Figure 22b shows that the external quantum efficiency exceeds 96% on the whole relevant wavelength range, and even values higher than 100% are obtained in the ultraviolet range. This above unity response with high-energy photons can be explained by secondary ionization [89]. For comparison, two state-of-the-art photodiodes optimized either to near ultraviolet (UV) or infrared (IR) range [90] and the best nanostructured pn-junction photodiode reported so far [91] (see Figure 22) were chosen. In the UV-range (< 400 nm), which is well-known to be challenging for conventional photodiodes [92], the spectral response of the b-Si device clearly exceeds the responses of all of the reference devices. The violet enhanced S3590 photodiode, which is tailored for near ultraviolet range, achieves a comparable light response only at a very narrow wavelength region around 400 nm due to conventionally optimized antireflection. At wavelengths above 500 nm all the way to 950 nm the b-Si photodiode is noticeably more sensitive than the reference devices, outperforming even the IR-optimized S11499 photodiode. The best nanostructured pn-junction photodiode reported so far has much lower response than any of the other photodiodes. This is probably due to damage created during laser processing, Auger recombination and insufficient surface passivation. Regarding external quantum efficiency, the previously reported photodiodes typically stay far below 90% as the b-Si photodiode reaches above 96%.

The demonstrated increase of photodiode quantum efficiency to above 96% gives direct benefits to practically all applications where detection of light is needed. This includes also devices where the measured quantity is converted to light *e.g.* via a scintillator. The applications range from camera shutter controls through fiber optic links, blood particle analyzers and encoders to airport X-ray security scanners. Improved sensitivity can reduce the amount of light needed in the process, decrease the size of the detector, or increase the signal level keeping everything else the same. Alternatively, a smaller, lighter and cheaper device can be realized. Other examples are security and medical imaging, where improved sensitivity can reduce the amount of radiation required for a certain image quality. Therefore, less power and radiation protective materials are needed, the X-ray gun and related power sources can be made smaller etc. Alternatively, better images can be acquired or luggage scanners operated faster. Additionally, the above and many other applications require measurement of diffuse light, in which the wide acceptance angle will further enhance the superior signal level compared to current planar photodiodes.

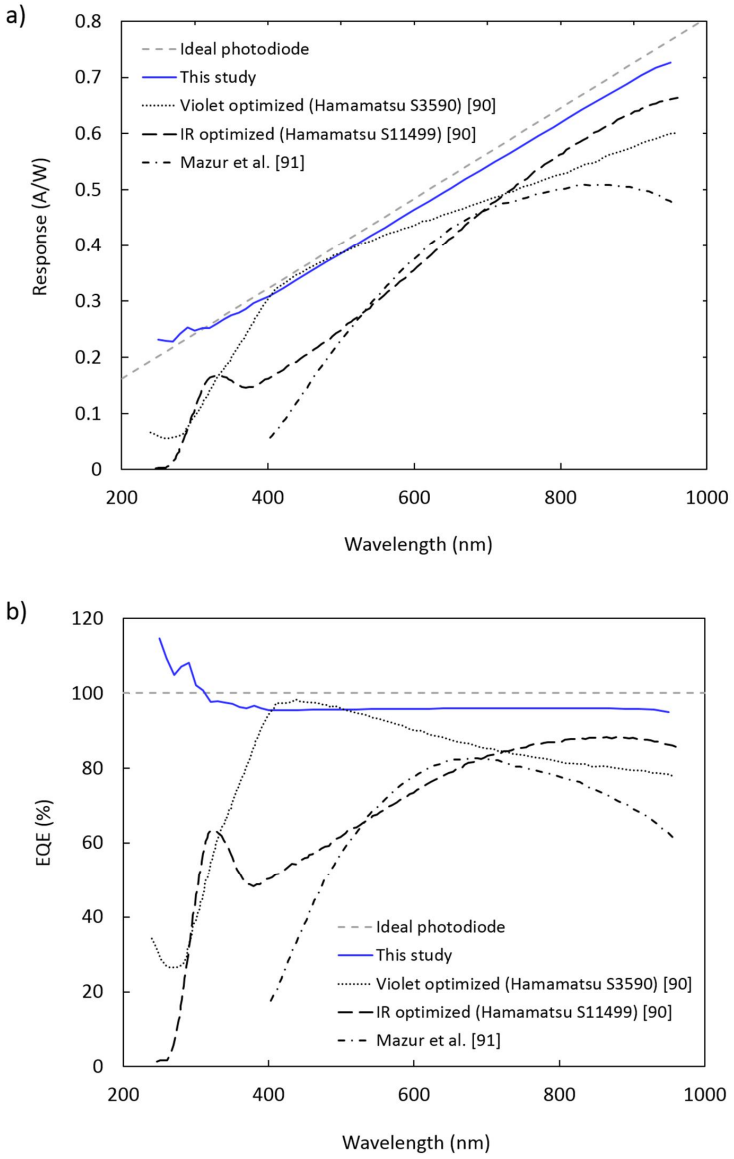

Figure 22. *a) Measured spectral light response of the b-Si photodiode compared to commercially available violet and infrared optimized photodiodes from Hamamatsu [90]. Comparison with the currently best nanostructured photodiode from Mazur et al. [91] is also included. Gray dashed line indicates the response of an ideal photodiode with 100% EQE. b) The corresponding EQE curves calculated from the spectral responses.*

5. Conclusions

This work examined the reduction of two eminent losses in silicon solar cells: surface recombination and surface reflectance. First, surface passivation of silicon with different ALD thin films was addressed. Al_2O_3 provided good surface passivation that is dependent on the oxidant used. The best results were reached with Al_2O_3 doped with TiO_2 that resembles an $(Al_2O_3)_x(TiO_2)_{1-x}$ alloy [22]. AlN and HfO_2 were introduced as alternative ALD materials for surface passivation. In addition to surface passivation, both of these materials have the potential of acting as antireflection coatings as they can have high refractive indexes which is a clear benefit as compared to Al_2O_3. Depending on the oxidant used, HfO_2 exhibited excellent surface passivation with relatively high negative fixed charge and refractive index of 2.1. AlN provided moderate surface passivation with good interface quality. To reach excellent surface passivation on lowly doped p-type silicon an additional corona charging was required. More thorough analysis regarding *e.g.* the interfaces, chemical composition and structure of both AlN and HfO_2 films would help to explain and fully understand the main mechanisms behind the surface passivation with these materials.

Second main theme of this thesis was the reduction of surface reflectance by nanostructurization. Furthermore, ALD Al_2O_3 surface passivation that was studied first on planar surfaces was applied also on black silicon where high surface recombination velocity due to increased surface area has been limiting its application. It was shown that issues with surface recombination on lowly doped p-type b-Si can be solved by ALD Al_2O_3 passivation. Black silicon also exhibited extremely low reflectance on a wide spectral range, even lower than 1%. It was demonstrated that the use of different oxidants in the ALD process can affect surface passivation of b-Si. Best results were achieved using H_2O whereas using O_3 or the combined process of H_2O+O_3 lead to lower lifetimes in b-Si. The trend was opposite in the case of planar samples: best surface passivation was reached with O_3-based processes.

As the next step towards actual solar cells, black silicon passivation was demonstrated on highly boron dopes emitters. The emitter formation and subsequent processing steps did not have a noticeable effect on the black silicon structure and the excellent optical properties remained. The fact that not even the drive-in oxidation after boron diffusion was harmful for black silicon enables optimization of the emitter profile. Simulations indicated that all the used diffusion processes lead to complete doping of the nanostructure and planar junction underneath it. Most importantly, good surface passivation with Al_2O_3 was reached also on p+ emitters.

As excellent Al_2O_3 passivation on lowly and highly doped p-type b-Si surfaces was achieved, both were applied on device level. An efficiency of 18.7% was achieved on n-type PERL solar cells with boron doped emitters, black silicon surface texture and Al_2O_3 front surface passivation. This was the highest b-Si solar cell efficiency during its time of publication although few problems hindering the efficiency were identified. *PassDop* rear

surface passivation was not compatible with the used substrate and the annealing temperature that was needed to activate Al_2O_3 surface passivation. These issues can be avoided by adjusting the solar cell process accordingly. The evaporated contacts showed poor conformality on b-Si that could be improved by optimizing the metallization process or by changing the cell structure to such that the surface underneath the contacts is flat.

To completely avoid problems with contact formation an interdigitated back-contact solar cell with b-Si and Al_2O_3 front surface was introduced. An efficiency of 22.1% was reached with these cells and the previously reported efficiency record was further improved. In addition to the avoidance of contact formation on b-Si another significant difference between front contact and rear contact cells can improve the efficiency in the latter: there is no need for emitter formation on the front surface and hence the Auger recombination there can be avoided. Further improvements for also the IBC cells to reach even higher efficiencies were discussed. It was shown that the b-Si IBC cells can perform better as compared to random pyramid textured reference cells when light enters the cell from low angles. The calculated yearly production of b-Si cells outperformed the reference cells regardless of the latitude, the increase being even more pronounced far from the equator.

Finally, the b-Si process was also applied on induced junction photodiodes. An inversion layer and hence a collecting junction was created with the negative fixed charge of Al_2O_3 on high resistivity n-type Si. Al_2O_3 also provided excellent b-Si front surface passivation. In this application low reflectance ensures that smaller amounts of light entering also from wider angles can be detected. Quantum efficiency above 96% and near-unity response on a wide wavelength range were reported. This gives direct benefits to practically all applications where detection of light is needed.

The excellent surface passivation and low reflectance results presented here prove the potential of using the combination of black silicon and ALD Al_2O_3 in different photovoltaic devices. Solar cells and photodiodes on a laboratory scale have shown good performance and with more process optimization even better could be expected. Also, there is a great promise to bring black silicon from the lab to industry in the near future due to its strong resilience to multiple processing steps demonstrated in this thesis.

References

[1] A. Aberle, Overview on SiN surface passivation of crystalline silicon solar cells, Solar Energy Materials & Solar Cells 65, 239-248 (2001).

[2] Y. Tsunomura, T. Yoshimine, M. Taguchi, T. Baba, T. Kinoshita, H. Kanno, H. Sakata, E. Maruyama, and M. Tanaka, Twenty-two percent efficiency HIT solar cell, Solar Energy Materials & Solar Cells 93, 670-673 (2009).

[3] O. Schultz, A. Mette, M. Hermle, and S. W. Glunz, Thermal oxidation for crystalline silicon solar cells exceeding 19% efficiency applying industrially feasible process technology, Progress in Photovoltaics: Research and Applications 16, 317-324 (2008).

[4] G. Dingemans and W. M. M. Kessels, Status and prospects of Al_2O_3-based surface passivation schemes for silicon solar cells, Journal of Vacuum Science and Technology A 30, 040802 (2012).

[5] G. Dingemans and W. M. M. Kessels, Aluminum oxide and other ALD materials for Si surface passivation, *ECS Transactions* **41**, 293-301 (2011).

[6] A. ur Rehman and S.H. Lee, Advancements in n-type base crystalline silicon solar cells and their emergence in the photovoltaic industry, *The Scientific World Journal* **2013**, (2013).

[7] S. Mack, A. Wolf, C. Brosinsky, S. Schmeisser, A. Kimmerle, P. Saint-Cast, M. Hofmann, and D. Biro, Silicon surface passivation by thin thermal oxide/PECVD layer stack systems, *Journal of Photovoltaics* **1**, 135-145 (2011).

[8] J. M. Khoshman, A. Khan, M.E. Kordesch, Amorphous hafnium oxide thin films for antireflection optical coatings, *Surface & Coatings Technology* **202**, 2500–2502 (2008).

[9] D. Hocine, M. S. Belkaid, M. Pasquinelli, L. Escoubas, J. J. Simon, G. A. Rivière, and A. Moussi, Improved efficiency of multicrystalline silicon solar cells by TiO_2 antireflection coatings derived by APCVD process, *Materials Science in Semiconductor Processing* **16**, 113-117 (2013).

[10] R. B. Wehrspohn, U. Rau, and A. Gombert, Photon Management in Solar Cells, (John Wiley & Sons, 2015) pp. 137.

[11] L. Sainiemi, K. Grigoras, and S. Franssila, Suspended nanostructured alumina membranes, *Nanotechnology* **20**, 075306 (2009).

[12] G. Agostinelli, A. Delabie, P. Vitanov, Z. Alexieva, H. F. W. Dekkers, S. De Wolf, and G. Beaucarne, Very low surface recombination velocities on p-type silicon wafers passivated with a dielectric with fixed negative charge, *Solar Energy Materials & Solar Cells* **90**, 3438-3443 (2006).

[13] B. Hoex, J. Schmidt, P. Pohl, M. C. M. van de Sanden, and W. M. M. Kessels, On the c-Si surface passivation mechanism by the negative-charge dielectric Al_2O_3, *Journal of Applied Physics* **104**, 044903 (2008).

[14] B. Hoex, M. C. M. van de Sanden, J. Schmidt, R. Brendel, and W. M. M. Kessels, Surface passivation of phosphorus-diffused n+-type emitters by plasma-assisted atomic layer deposited Al_2O_3, *Physica Status Solidi RRL* **6**, 4–6 (2012).

[15] G. Dingemans, M.C.M. van de Sanden, and W.M.M. Kessels, Influence of the deposition temperature on the c-Si surface passivation by Al_2O_3 films synthesized by ALD and PECVD, *Electrochemical and Solid-State Letters* **13**, H76-H79 (2010).

[16] G. Dingemans, R. Seguin, P. Engelhart, M.C.M. van de Sanden, and W.M.M. Kessels, Silicon surface passivation by ultrathin Al_2O_3 films synthesized by thermal and plasma atomic layer deposition, *Physica Status Solidi RRL* **4**, 10-12 (2010).

[17] J. Schmidt, B. Veith, F. Werner, D. Zielke, and R. Brendel, Silicon surface passivation by ultrathin Al_2O_3 films and Al_2O_3/SiN_x stacks, in *Proceedings of the 35th IEEE Photovoltaic Specialists Conference*, (Honolulu, HI, USA, 2010) pp. 885-890.

[18] S. Li, Y. Bao, M. Laitinen, T. Sajavaara, M. Putkonen, and H. Savin, Excellent silicon surface passivation using dimethylaluminiumchloride as Al source for atomic layer deposited Al_2O_3, *Physica Status Solidi A* **212**, 1795–1799 (2015).

[19] H. Kato, K. S. Seol, M. Fujimaki, T. Toyoda, Y. Ohki, and M. Takiyama, Effect of ozone annealing on the charge trapping property of Ta_2O_5–Si_3N_4-p–Si capacitor grown by low-pressure chemical vapor deposition, *Japanese Journal of Applied Physics* **38**, 6791–6796 (1999).

[20] S. Jakschik, U. Schroeder, T. Hecht, D. Krueger, G. Dollinger, A. Bergmaier, C. Luhmann, J.W. Bartha, Physical characterization of thin ALD- Al_2O_3 films, *Applied Surface Science* **211**, 352–359 (2003).

[21] G. von Gastrow, S. Li, M. Putkonen, M. Laitinen, T. Sajavaara, and H. Savin, Effect of ozone concentration on silicon surface passivation by atomic layer deposited Al_2O_3, *Applied Surface Science* **357**, 2402-2407 (2015).

[22] P. Vitanov, G. Agostinelli, A. Harizanova, T. Ivanova, M. Vukadinovic, N. Le Quang, and G. Beaucarne, Low cost surface passivation for p-type mc-Si based on pseudobinary alloys $(Al_2O_3)_x(TiO_2)_{1-x}$, *Solar Energy Materials & Solar Cells* **90**, 2489-2495 (2006).

[23] B. Vermang, H. Goverde, A. Lorenz, A. Uruena, G. Vereecke, J. Meersschaut, E. Cornagliotti, A. Rothschild, J. John, J. Poortmans, and R. Mertens1, On the blistering of atomic layer deposited Al_2O_3 as Si surface passivation, in *Proceedings of the 37th IEEE Photovoltaic Specialists Conference* (Seattle, WA, USA, 2011), pp. 003562-003567.

[24] B. Liao, B. Hoex, A. G. Aberle, D. Chi, and C. S. Bhatia, Excellent c-Si surface passivation by low-temperature atomic layer deposited titanium oxide, *Applied Physics Letters* **104**, 253903 (2014).

[25] J. Gope, Vandana, N. Batra, J. Panigrahi, R. Singh, K.K. Maurya, R. Srivastava, and P.K. Singh, Silicon surface passivation using thin HfO_2 films by atomic layer deposition, *Applied Surface Science* **357**, 635-642 (2015).

[26] T. G. Allen and A. Cuevas, Electronic passivation of silicon surfaces by thin films of atomic layer deposited gallium oxide, *Applied Physics Letters* **105**, 031601 (2014).

[27] Y. Wan, J. Bullock, and A. Cuevas, Tantalum oxide/silicon nitride: A negatively charged surface passivation stack for silicon solar cells, *Applied Physics Letters* **114**, 174301 (2013).

[28] B.W.H. van de Loo, H. C. M. Knoops, G. Dingemans, G. J. M. Janssen, M. W. P. E. Lamers, I. G. Romijn, A. W. Weeber, and W. M. M. Kessels, "Zero-charge" SiO_2/ Al_2O_3 stacks for the simultaneous passivation of n+ and p+ doped silicon surfaces by atomic layer deposition, *Solar Energy Materials and Solar Cells* **143**, 450-456 (2015).

[29] B. G. Lee, S. Li, G. von Gastrow, M. Yli-Koski, H. Savin, V. Malinen, J. Skarp, S. Choi, and H. M. Branz, Excellent passivation and low reflectivity with atomic layer deposited bilayer coatings for n-type silicon solar cells, *Thin Solid Films* **550**, 541–544 (2014).

[30] D. K. Simon, P. M. Jordan, T. Mikolajick, and I. Dirnstorfer, On the control of the fixed charge densities in Al_2O_3 based silicon surface passivation schemes, *ACS Applied Materials & Interfaces* **7**, 28215−28222 (2015).

[31] K.-C. Huang, P.-Y. Chen, R. Vittal, and K.-C. Ho, Enhanced performance of a quasi-solid-state dye-sensitized solar cell with aluminum nitride in its gel polymer electrolyte, *Solar Energy Materials and Solar Cells* **95**, 1990-1995 (2011).

[32] M. Bosund, P. Mattila, A. Aierken, T. Hakkarainen, H. Koskenvaara, M. Sopanen, V.-M. Airaksinen, and H. Lipsanen, GaAs surface passivation by plasma-enhanced atomic-layer-deposited aluminum nitride, *Applied Surface Science* **256**, 7434-7437 (2010).

[33] M. M. De Souza, S. Jejurikar, and K. P. Adhi, Impact of aluminum nitride as an insulator on the performance of zinc oxide thin film transistors, *Applied Physics Letters* **92**, 093509 (2008).

[34] P. M. Kaminski, K. Bass, and G. Claudio, High bandgap dielectrics for antireflective coating in silicon solar cells by reactive ion sputtering, *Physica Status Solidi C* **8**, 1311-1314 (2011).

[35] G. Krugel, F. Jenkner, A. Moldovan, W. Wolke, J. Rentsch, and R. Preu, Investigations on the passivation mechanism of AlN:H and AlN:H-SiN:H stacks, *Energy Procedia* **55**, 797 – 804 (2014).

[36] M. Wilson, J. Lagowski, L. Jastrzebski, A. Savtchouk, and V. Faifer, COCOS (corona oxide characterization of semiconductor) non-contact metrology for gate dielectrics, in *AIP Conference Proceedings* (Gaithersburg, MD, USA, 2001), pp. 220-225.

[37] T. Mattila and R. M. Nieminen, Point-defect complexes and broadband luminescence in GaN and AlN, *Physical Review B* **55**, 9571-9576 (1997).

[38] User manual, PV 2000A Spesifications, Semilab (2014).

[39] G. D. Wilk, R. M. Wallace, and J. M. Anthony, High-κ gate dielectrics: Current status and materials properties considerations, *Journal of Applied Physics* **89**, 5243 (2001).

[40] F. Lin, B. Hoex, Y. H. Koh, J. Lin, and A. G. Aberle, Low-temperature surface passivation of moderately doped crystalline silicon by atomic-layer-deposited hafnium oxide films, *ECS Journal of Solid State Science and Technology* **2**, N11-N14 (2013).

[41] J. Wang, S. S. Mottaghian, and M. F. Baroughi, Passivation properties of atomic-layer-deposited hafnium and aluminum oxides on Si surfaces, *IEEE Transactions on Electron Devices* **59**, 342-348 (2012).

[42] A. Morato, B. Vermang, H. Goverde, E. Cornagliotti, G. Meneghesso, J. John, and J. Poortmans, Electrical characterization of ALD Al_2O_3-HfO_2 and PECVD Al_2O_3 passivation layers for p-type CZ-Silicon PERC solar cells, in *Proceedings of 38th IEEE Photovoltaic Specialists Conference* (Austin, TX, USA, 2012), pp. 220-225.

[43] R. Sreenivasan, P. C. McIntyre, H. Kim, and K. C. Saraswat, Effect of impurities on the fixed charge of nanoscale HfO_2 films grown by atomic layer deposition, *Applied Physics Letters* **89**, 112903 (2006).

[44] H. García, H. Castán, S. Dueñas, L. Bailón, F. Campabadal, O. Beldarrain, M. Zabala, M. B. González, and J. M. Rafí, Electrical characterization of atomic-layer-deposited hafnium oxide films from hafnium tetrakis(dimethylamide) and water/ozone: Effects of growth temperature, oxygen source, and postdeposition annealing, *Journal of Vacuum Science & Technology A* **31**, 01A127 (2013).

[45] J. Fan, H. Liu, Q. Kuang, B. Gao, F. Ma, and Y. Hao, Physical properties and electrical characteristics of H_2O-based and O_3-based HfO_2 films deposited by ALD, *Microelectronics Reliability* **52**, 1043–1049 (2012).

[46] P. S. Lysaght, B. Foran, G. Bersuker, P. J. Chen, R. W. Murto, and H. R. Huff, Physicochemical properties of HfO_2 in response to rapid thermal anneal, *Applied Physics Letters* **82**, 1266 (2003).

[47] J. Lu, J. Aarik, J. Sundqvist, K. Kukli, A. Hårsta, J.-O. Carlsson, Analytical TEM characterization of the interfacial layer between ALD HfO_2 film and silicon substrate, *Journal of Crystal Growth* **273**, 510-514 (2005).

[48] J. Li, H. Y. Yu, and Y. Li, Aligned Si nanowire-based solar cells, *Nanoscale* **3**, 4888-4900 (2011).

[49] L. Sainiemi, V. Jokinen, A. Shah, M. Shpak, S. Aura, P. Suvanto, and S. Franssila, Non-reflecting silicon and polymer surfaces by plasma etching and replication, *Advanced Materials* **23**, 122-126 (2011).

[50] H.-C. Yuan, V. E. Yost, M. R. Page, P. Stradins, D. L. Meier, and H. M. Branz, Efficient black silicon solar cell with a density-graded nanoporous surface: Optical properties, performance limitations, and design rules, Applied Physics Letters **95**, 123501 (2009.)

[51] S. Koynov, M. S. Brandt, and M. Stutzmann, Black multi-crystalline silicon solar cells, *Physica Status Solidi RRL* **1**, R53-R55 (2007).

[52] Y. Yan, H.-C. Yuan, V. E. Yost, K. Jones, M. Al-Jassim, and H. M. Branz, Microstructure and surface chemistry of nanoporous "black silicon" for photovoltaics, in *Proceedings of the 35th IEEE Photovoltaic Specialists Conference* (Honolulu, HI, USA, 2010), pp. 2255-2257.

[53] F. Toor, H. M. Branz, M. R. Page, K. M. Jones, and H.-C. Yuan, Multi-scale surface texture to improve blue response of nanoporous black silicon solar cells, *Applied Physics Letters* **99**, 103501 (2011).

[54] C.-H. Lin, D. Z. Dimitrov, C.-H. Du, and C.-W. Lan, Influence of surface structure on the performance of black-silicon solar cell, *Physica Status Solidi* **C 7**, 2778-2784 (2010).

[55] P. B. Clapham and M. C. Hutley, Reduction of lens reflexion by the "moth-eye" principle, *Nature* **244**, 281-282 (1973).

[56] A. J. Bett, J. Eisenlohr, O. Höhn, P. Repo, H. Savin, B. Bläsi, and J. C. Goldschmidt, Wave optical simulation of the light trapping properties of black silicon surface textures, *Optics Express* **24**, A434-A445 (2016).

[57] M. Otto, M. Algasinger, H. Branz, B. Gesemann, T. Gimpel, K. Füchsel, T. Käsebier, S. Kontermann, S. Koynov, X. Li, V. Naumann, J. Oh, A. N. Sprafke, J. Ziegler, M. Zilk, and R. B. Wehrspohn, Black Silicon Photovoltaics, *Advanced Optical Materials* **3**, 147–164 (2015).

[58] S. Koynov, M. S. Brandt, and M. Stutzmann, Black nonreflecting silicon surfaces for solar cells, *Applied Physics Letters* **88**, 203107 (2006).

[59] M. Halbwax, T. Sarnet, P. Delaporte, M. Sentis, H. Etienne, F. Torregrosa, V. Vervisch, I. Perichaud, and S. Martinuzzi, Micro and nano-structuration of silicon by femtosecond laser: Application to silicon photovoltaic cells fabrication, *Thin Solid Films* **516**, 6791-6795 (2008).

[60] V. Lehmann, The physics of macropore formation in low doped n-type silicon, *Journal of Electrochemical Society* **140**, 2836-2843 (1993).

[61] Y. Xia, B. Liu, J. Liu, Z. Shen, and C. Li, A novel method to produce black silicon for solar cells, *Solar Energy* **85**, 1574–1578 (2011).

[62] X. Liu, P. R. Coxon, M. Peters, B. Hoex, J. M. Cole, and D. J. Fray, Black silicon: fabrication methods, properties and solar energy applications, *Energy & Environmental Science* **7**, 3223-3263 (2014).

[63] C.-H. Hsu, J.-R. Wu, Y.-T. Lu, D. J. Flood, A. R. Barron, L.-C. Chen, Fabrication and characteristics of black silicon for solar cell applications: An overview, *Materials Science in Semiconductor Processing* **25**, 2-17 (2014).

[64] H. Jansen, M. de Boer, R. Legtenberg, and M. Elwenspoek, The black silicon method: a universal method for determining the parameter setting of a fluorine-based reactive ion etcher in deep silicon trench etching with profile control, *Journal of Micromechanics and Microengineering* **5**, 115–120 (1995).

[65] G. von Gastrow, R. Alcubilla, P. Ortega, M. Yli-Koski, S. Conesa-Boj, A. Fontcuberta i Morral, and H. Savin, Analysis of the atomic layer deposited Al_2O_3 field-effect passivation in black silicon, *Solar Energy Materials & Solar Cells* **142**, 29-33 (2015).

[66] H. V. Jansen, M. J. de Boer, K. Ma, M. Girones, S. Unnikrishnan, M. C. Louwerse, and M. C. Elwenspoek, Black silicon method XI: oxygen pulses in SF_6 plasma, *Journal of Micromechanics and Microengineering* **20**, 075027 (2010).

[67] M. Köhler, Etching in Microsystems Technology (Wiley-VCH, Weinheim, 1999) pp. 162–163.

[68] R Dussart, T. Tillocher, P. Lefaucheux, and M. Boufnichel, Plasma cryogenic etching of silicon: from the early days to today's advanced technologies, *Journal of Physics D: Applied Physics* **47**, 123001 (2014).

[69] M. Steglich, T. Käsebier, M. Zilk, T. Pertsch, E.-B. Kley, and A. Tünnermann, The structural and optical properties of black silicon by inductively coupled plasma reactive ion etching, *Journal of Applied Physics* **116**, 173503 (2014).

[70] J. Yoo, G. Yu, and J. Yi, Black surface structures for crystalline silicon solar cells, *Materials Science and Engineering B* **159–160**, 333–337 (2009).

[71] J. A. Giesecke, M. C. Schubert, D. Walter, and W. Warta, Minority carrier lifetime in silicon wafers from quasi-steady-state photoluminescence, *Applied Physics Letters* **97**, 092109 (2010).

[72] P. Repo, A. Haarahiltunen, M. Yli-Koski, H. Talvitie, L. Sainiemi, M. C. Schubert, and H. Savin, Passivation of black silicon surfaces with ALD Al_2O_3, in *2nd International Conference on Silicon Photovoltaics, SiliconPV* (3rd of April 2012, Leuven, Belgium). Presentation slides.

[73] M. Otto, M. Kroll, T. Käsebier, R. Salzer, A. Tünnermann, and R. B. Wehrspohn, Extremely low surface recombination velocities in black silicon passivated by atomic layer deposition, *Applied Physics Letters* **100**, 191603 (2012).

[74] Z. Xia, J. Dong, X. Li, C. Ren, R. Sidhu, W. Song, L.Tao, Z. Yangj, B. Zhang, and G. Xing, Comparison between passivation properties of thermal ALD Al_2O_3 deposited with TMA+O_3 and TMA+H_2O, in *Proceedings of the 38th IEEE Photovoltaic Specialists Conference* (Austin, TX, USA, 2012), pp. 001163–001165.

[75] J. Benick, B. Hoex, M. C. M. van de Sanden, W. M. M. Kessels, O. Schultz, and S. W. Glunz, High efficiency n-type Si solar cells on Al_2O_3-passivated boron emitters, *Applied Physics Letters* **92**, 253504 (2008).

[76] J. Benick, B. Hoex, G. Dingemans, A. Richter, M. Hermle and S. W. Glunz, High efficiency n-type Si solar cells on Al_2O_3-passivated boron emitters, in *Proceedings of the 24th European PV Solar Energy Conference and Exhibition* (Hamburg, Germany, 2009), pp. 863 – 870.

[77] Sentaurus Synopsys. (2012). Synopsys TCAD, release G 2012.06. Available: http://www.synopsys.com.

[78] J. Schön, A. Abdollahinia, R. Müller, J. Benick, M. Hermle, W. Warta, and M. C. Schubert, Predictive simulation of doping processes for silicon solar cells, *Energy Procedia* **38**, 312-320 (2013).

[79] A. Richter, J. Benick, and M. Hermle, Boron emitter passivation with Al_2O_3 and Al_2O_3/SiN_x stacks using ALD Al_2O_3, *Journal of Photovoltaics* **3**, 236-244 (2013).

[80] J. Oh, H.-C. Yuan, and H. M. Branz, An 18.2%-efficient black-silicon solar cell achieved through control of carrier recombination in nanostructures, Nature *Nanotechnology* **7**, 743-748 (2012).

[81] D. Suwito, U. Jäger, J. Benick, S. Janz, M. Hermle, and S. W. Glunz, Industrially feasible rear passivation and contacting scheme for high-efficiency n-type solar cells yielding a V_{oc} of 700 mV, *IEEE Transactions on Electron Devices* **57**, 2032-2036 (2010).

[82] P. Ortega, E. Calle, G. von Gastrow, P. Repo, D. Carriõ, H. Savin, and R. Alcubilla, High-efficiency black silicon interdigitated back contacted solar cells on p-type and n-type c-Si substrates, *Progress in Photovoltaics: Research and Applications* **23**, 1448–1457 (2015).

[83] M. J. de Boer, J. G. E. (H.) Gardeniers, H. V. Jansen, E. Smulders, M.-J. Gilde, G. Roelofs, J. N. Sasserath, and M. Elwenspoek, Guidelines for etching silicon MEMS structures using fluorine high-density plasmas at cryogenic temperatures, *Journal of Microelectromechanical Systems* **11**, 385-401 (2002).

[84] B. Gesemann, R. Wehrspohn, A. Hackner, and G. Müller, Large-scale fabrication of ordered silicon nanotip arrays used for gas ionization in ion mobility spectrometers, *IEEE Transactions on Nanotechnology* **10**, 50-52 (2011).

[85] P. Hoyer, M. Theuer, R. Beigang, and E.-B. Kley, Terahertz emission from black silicon, *Applied Physics Letters* **93**, 091106 (2008).

[86] L. Sainiemi, H. Keskinen, M. Aromaa, L. Luosujärvi, K. Grigoras, T. Kotiaho, J. M. Mäkelä, and S. Franssila, Rapid fabrication of high aspect ratio silicon nanopillars for chemical analysis, *Nanotechnology* **18**, 505303 (2007).

[87] Z. Huang, J. E. Carey, M. Liu, X. Guo, E. Mazur, and J. C. Campbell, Microstructured silicon photodetector, *Applied Physics Letters* **89**, 033506 (2006).

[88] M. Sildoja, F. Manoocheri, M. Merimaa, E. Ikonen, I. Müller, L. Werner, J. Gran, T. Kübarsepp, M. Smîd, and M. L. Rastello, Predictable quantum efficient

detector: I. Photodiodes and predicted responsivity, *Metrologia* **50**, 385-394 (2013).

[89] V. S. Vavilov, Effect of Radiation on Semiconductors (Springer Science, Business Media, New York, 1965).

[90] Hamamatsu Photonics, Opto-semiconductor 2014/CHAPTER 02_Si photodiodes, https://www.hamamatsu.com/resources/pdf/ssd/e02_handbook_si_photodiode.pdf

[91] E. Mazur, Laser doping and texturing of silicon for advanced optoelectronic devices, in *11th Conference on Lasers and Electro-Optics Pacific Rim* (25th of August 2015, Busan, South Korea,). Presentation slides.

[92] F. Guo, B. Yang, Y. Yuan, Z. Xiao, Q. Dong, Y. Bi, and J. Huang, A nanocomposite ultraviolet photodetector based on interfacial trap-controlled charge injection, *Nature Nanotechnology* **7**, 798-802 (2012).

Errata

Publication V

From equation $2 \times J_{0e}$ = fA/cm^2 value 102 is missing, *i.e.* $2 \times J_{0e} = 102$ fA/cm^2.

Aalto-DD 139/2016

ISBN 978-952-60-6918-0 (printed)
ISBN 978-952-60-6919-7 (pdf)
ISSN-L 1799-4934
ISSN 1799-4934 (printed)
ISSN 1799-4942 (pdf)

Aalto University
School of Electrical Engineering
Department of Micro- and Nanosciences
www.aalto.fi

BUSINESS + ECONOMY

ART + DESIGN + ARCHITECTURE

SCIENCE + TECHNOLOGY

CROSSOVER

DOCTORAL DISSERTATIONS